

A systematic approach for enhancement of homogeneous background images using structural information

D. Vijayalakshmi ^{a,*}, Malaya Kumar Nath ^b

^a Department of ECE, Vignan's Institute of Engineering for Women, Visakhapatnam, Andhra Pradesh, India

^b Department of ECE, National Institute of Technology Puducherry, Karaikal, Puducherry, India



ARTICLE INFO

Keywords:

Rènyi entropy

Uniform background images

Structural information

Sub-histogram equalization

Contrast enhancement

ABSTRACT

Image enhancement is an indispensable pre-processing step for several image processing applications. Mainly, histogram equalization is one of the widespread techniques used by various researchers to improve the image quality by expanding the pixel values to fill the entire dynamic grayscale. It results in the visual artifact, structural information loss near edges due to the information loss (due to many-to-one mapping), and alteration in average luminance to a higher value. This paper proposes an enhancement algorithm based on structural information for homogeneous background images. The intensities are divided into two segments using the median value to preserve the average luminance. Unlike traditional techniques, this algorithm incorporates the spatial locations in the equalization process instead of the number of intensity values occurrences. The occurrences of each intensity concerning their spatial locations are combined using Rènyi entropy to enumerate a discrete function. An adaptive clipping limit is applied to the discrete function to control the enhancement rate. Then histogram equalization is performed on each segment separately, and the equalized segments are integrated to produce an enhanced image. The algorithm's effectiveness is validated by evaluating the proposed method on CEED, CSIQ, LOL, and TID2013 databases. Experimental results reveal that the proposed method improves the contrast while preserving structural information, detail information, and average luminance. They are quantified by the high value of contrast improvement index, structural similarity index, and discrete entropy, and low value of average mean brightness error values of the proposed method when compared with the methods available in the literature, including deep learning architectures.

1. Introduction

Images are the most commonly used medium for conveying or exchanging information. They are mostly utilized in engineering applications that need a passive or non-contact perception for the working environment such as remote sensing images [1,2], industrial monitoring [3], video and aerial surveillance [4,5], object detection [6], tracking [7], medical diagnosis [8], and so on. During image acquisition process, the captured images are usually affected by light scattering and absorption, resulting in low contrast and blurry images [9]. These images conceal valuable information thereby limiting the applications supported by them. So, it is required to examine image processing algorithms to identify their concealed information. The collegiate of these algorithms are referred as image enhancement. Image enhancement refers to the procedures that improve the appearance of an image to a human viewer or operations that transform an image to a format that

is better suited for machine processing. Generally, image enhancement can be done either by improving the contrast or removing the noise from it.

The contrast enhancement (CE) techniques are classified based on various factors. Based on the operation domain, they are classified into spatial domain and temporal domain techniques [10]. The temporal domain methods require parameter tuning for the enhancement process. The spatial domain methods needs less number of tunable parameters compared to the temporal domain methods. Due to the above-mentioned reason spatial domain methods are preferable for the CE process. Histogram based and retinex based methods are part of classifications of the spatial domain methods [11]. Due to the development in technology, computer vision applications have gained popularity. Artificial intelligence plays a vital role in all autonomous applications like medical diagnostics and remote sensing. Deep learning based algorithms are also developed for the purpose of contrast improvement. Most of the deep learning architectures are developed

* Corresponding author.

E-mail addresses: vijaya1183@gmail.com (D. Vijayalakshmi), malaya.nath@nitp.ac.in (M.K. Nath).

based on consideration of image as a combination of illumination and reflectance components.

1.1. Motivation and contribution

Improving the contrast is achieved by incrementing the difference amid the pixel and its neighborhood [12]. The characteristic of the pixel is obtained from its neighborhood. It might be helpful to fix the level of enhancement for the particular pixel and it urges us to utilize the spatial information in the equalization process to reduce the artifacts caused due to processing [13].

Brightness shifting and over enhancement causes major artifacts on the processed images produced by the contrast enhancement algorithms [14]. Maintaining the mean brightness aids to preserve the enhanced images from the artifacts caused by the display devices, and controlling the enhancement rate avoids the halo artifacts produced by the histogram spikes near the edges. Large uniform background images are mostly affected by the over enhancement and mean brightness shifting due to the presence of histogram spikes [15]. In this research, an algorithm is developed to improve the contrast of the large uniform background images while preserving the mean brightness and controlling the enhancement rate.

The proposed method solves the issue of over-enhancement by employing the steps mentioned below, which represent the significance of this work.

- Artifacts produced due to the shifting of mean brightness is reduced by employing the segmentation of intensities using the statistical parameter median.
- Incorporation of spatial information using Rényi entropy in the equalization process aids to improve the contrast based on the nature of the pixels.
- Reduction of over enhancement using the calculation of adaptive clipping limits due to the presence of histogram peaks.
- Preservation of information content by integrating the local contrast improvement in the discrete cosine transform domain (DCT).
- Computation of reference and non-reference metrics for validating the visual analysis of the efficacy of the suggested technique in comparison to conventional algorithms and neural network architectures.

The remaining sections are as follows: In Section 2, a literature review of spatial domain improvement techniques is presented. The methodology suggested is outlined in Section 3. Section 4 provides a summary of the experimental investigation of the proposed technique compared to numerous existing contrast enhancement algorithms. Section 5 concludes the paper.

2. Related work

A detail analysis is carried out on some of the existing histogram based, retinex based, and deep learning based existing contrast enhancement techniques and it is presented in this Section. Due to its simplicity, histogram equalization is a widely used contrast enhancement technique. Global histogram equalization (GHE) methods improve the overall image [16]. Improvement in local features of an image is needed in some cases as these features contribute the detail about local neighborhood. So it is performed by local histogram equalization, which equalizes a small segment of the histogram to enhance additional image features [17]. The number of gray levels is lowered in this process to increase the contrast between the intensity levels that differentiate the items. However, decreasing the intensity results in information loss. HE expands the intensities in accordance with their occurrences to fill the entire dynamic scale; this results in the difficulty of shifting the mean brightness to the dynamic scale's center.

This attribute of HE is incompatible with the display of enhanced images on consumer electronic gadgets. Bi-histogram equalization (BHE) approaches are created to address the above-stated issues [18,19].

BHE segments the histogram into two using the statistical parameters calculated from the low contrast image. Then the segments are equalized individually to produce an enhanced image. Recursive segmentation of histogram leads to preserve the average luminance more precisely [20]. But fixing the level of segmentation is critical because more number of histogram division results in an enhanced image which is similar to the low contrast input image. Additionally, bi-histogram approaches are created to manage the pace of amplification and mitigate the effect of intensity saturation [21]. Histogram clipping is employed to reduce the effect of intensity saturation. Generally mean, median, and entropy values are served as threshold values to perform histogram clipping in most of the existing BHE methods in the literature. Later, the clipping limits are calculated adaptively [22]. These methods generally suffered from the problem of little or no improvement in the amount of perceived contrast [23,24]. This could be a result of insufficient use of the entire dynamic scale. While the algorithms are built with a variety of purposes, such as structural information preservation, detail preservation, and entropy preservation. Greater emphasis should be placed on the fundamental objective of contrast enhancement.

Two-dimensional histogram-based methods are designed with the purpose of enhancing the spatial neighborhood information [25]. The neighborhood data assists in identifying the flat and edge detail in the images. Thus, while the 2D-based algorithms improve perceived contrast, there is no control over the augmentation rate, which results in over-enhancing [26]. Additionally, the quantity of mean brightness shifting is increased [27,28]. While developing 2D-based approaches, parameters should be devised to ensure that the AMBE is kept to a minimum and that the augmentation is controlled [29,30].

Enhancement methods based on retinex theory have been proposed to preserve the processed image's naturalness and its color information. Most of the retinex models remove the illumination component while processing the reflectance part of the given image to produce enhanced results. Removing the illumination for the dark pictures leads to artifacts in the processed images. The illumination part of the image is modified by the light map generated from the low light image to reduce the effects caused by its removal [31]. Then, improved results have been obtained by processing the simultaneous reflection and the illumination part of the low light images [32]. The works mentioned above have used simple priors to estimate various components of the given image, which results in an unnatural appearance in the improved image. Illumination based method (LIME) first focused on lighting estimation, which used edge-aware smoothing to improve the initial lighting map for processing both (illumination and reflectance) components [33]. The main drawback of LIME is that it is difficult to avoid getting too much exposure during the enhancement. It also requires post-processing for the artifact-free resultant image. In addition, the technique in [34,35] (STRU) proposed a denoising-type approach to simultaneously estimate light and reflectance because noises and artifacts may accompany the estimated reflectance.

Big data has led to a new trend: learning the distribution of data from a large number of training pairs in order to specify desired regularization. It has made significant progress in a number of vision-related fields [36–38]. For a task to be learned deeply, data is the most important aspect. It is becoming increasingly easy to get training data, thus classic image processing methods (such as super-resolution and dehazing) are practically completely occupied by deep learning. Low-light image enhancement training pairs are scarce in both synthetic and real imaging simulations, unlike the other tasks. There is a restriction on the growth of deep learning in this task. RetinexNet [39], a Retinex-based network, was created by Chen to simultaneously estimate the light and reflectance of a LOL dataset. In addition to a network for adjusting the illumination, they also provided a network for restoring the achieved

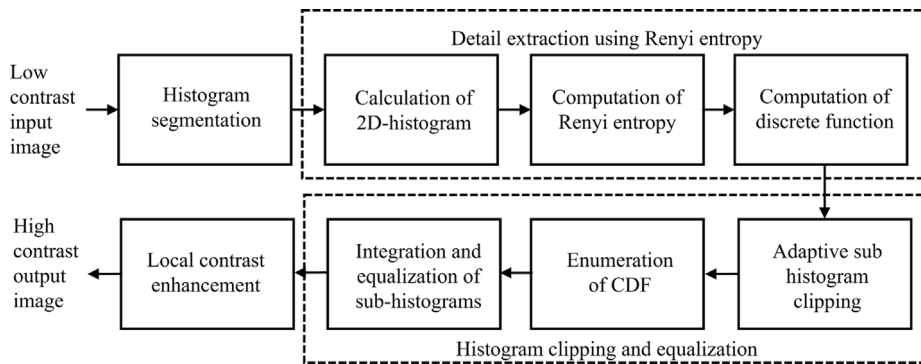


Fig. 1. Proposed block diagram for contrast enhancement.

reflectance in order to improve it even further. LightenNet (LLnet) [40] was built using a convolutional neural network to improve images that are under-exposed or over-exposed. Given the complexity and unreliability of data gathering, [41] developed EnlightenGAN (EGAN), an unsupervised generative adversarial network. Due to GAN's capability, this approach does not require the generation of a training dataset in low/normal light. Works without illumination focused exclusively on the construction of the mapping from observations or data. They made no reference to the application or modeling of physical principles. As a result, they are unable to efficiently handle the majority of low-light settings [42].

Contrast enhancement techniques can be developed to improve contrast while minimizing mean brightness shift, preserving structural information, and reducing intensity compression and saturation. However, several of the aforementioned aims are mutually exclusive. For instance, if the method results in least amount of brightness shifting, the degree of contrast enhancement is reduced. Similarly, if the technique is intended to maintain structural information, variations in the intensity levels around the edges should be minimal. While structural information is necessary for locating the region of interest in the augmented image, the transformation function alters the intensity levels towards the edges, so obliterating structural information [43,44]. As a result, building a multi-objective contrast enhancement algorithm is the solution to overcome the above-said limitations. In this paper, the proposed algorithm is developed based on two-dimensional histogram to produce a visually pleasing and an artifact-free enhanced images [45].

The following objectives are framed to develop contrast enhancement technique which helps to fulfill the motivation of the research.

1. Preservation of information content to assure the retention of gray levels in the processed image.
2. The unnatural appearance caused by over enhancement can be limited by controlling the enhancement rate.
3. Utilization of whole dynamic range of gray scale aids to differentiate various objects from the processed image.

The mathematical description of the proposed methodology is provided in Section 3.

3. Methodology

Fig. 1 shows the block diagram of the proposed Rènyi entropy based contrast enhancement. The mathematical description about each block is explained in the following sub sections.

3.1. Histogram segmentation

Consider an input image I with the size of $H \times W$. The pixel values of the considered image lie in the range of $[L_{min}, L_{max}]$. Here L_{min} and L_{max} denote the minimum and maximum pixel values of the image I , respectively. The histogram of the i th intensity is defined as number

of times the intensity i has been occurred in the given image. The following equation shows the calculation of the histogram

$$h_i = n_i \quad (1)$$

h_i denotes the histogram of the i^{th} intensity and n_i represents the number of occurrences of the intensity i .

Contrast enhancement procedure starts with histogram segmentation. Generally, low contrast and dark images are having skewed distribution of their pixel intensities in the entire dynamic gray scale. When compared to mean, the median is less susceptible to outliers and skewed data [46]. If the distribution is not symmetrical about the mean, then median is the preferable parameter to measure the central tendency of the data. From the literature, it is observed that median based bi-histogram equalization preserves the mean brightness and information content. Due to the above stated reasons, in this work median based segmentation is employed. The median value is computed by sorting the pixel intensities in ascending or descending then the middle value is found. It is denoted by L_{med} .

$$L_{med} = \text{median} ([L_{min}, L_{max}]) \quad (2)$$

The L_{med} divides the intensities into two segments, namely L_{s1} and L_{s2} . L_{s1} and L_{s2} represent the lower and upper segments, respectively.

$$L_{s1} = [L_{min}, L_{med} - 1] \quad (3)$$

$$L_{s2} = [L_{med}, L_{max}] \quad (4)$$

3.2. Calculation of 2D-histogram

After segmenting the intensity values, the 2D-histogram computed by dividing the whole image into number of spatial grids where the grids are not overlapped with each other. The total number of grids is represented as PQ and it is calculated from the number of distinct pixel values and the size of the considered image. Assume the number of distinct intensity value is represented as l then

$$P = \left\lfloor (l \times a_r)^{0.5} \right\rfloor, Q = \left\lfloor \left(\frac{l}{a_r} \right)^{0.5} \right\rfloor \quad (5)$$

Where ' P' ' and ' Q ' represent the size of the 2D histogram. It is calculated using the number of distinct intensities present in the image ' l ' and the aspect ratio ' a_r ' of the given image. $\lfloor \cdot \rfloor$ denotes the rounding of argument to the nearest integer. The aspect ratio ' a_r ' is calculated by

$$a_r = \frac{H}{W} \quad (6)$$

where H and W denote the number of rows and columns in the given image respectively. The size of the spatial grid is represented by $\frac{H}{P} \times \frac{W}{Q}$. The 2D-histogram is calculated using the equation represented below:

$$h_i = \{h_i(p, q) | 1 \leq p \leq P, 1 \leq q \leq Q\} \quad (7)$$

Table 1
Sample image I .

110	220	98	85	110	220	98	85
110	110	110	110	220	220	220	220
85	85	85	85	85	85	85	85
98	98	98	98	98	98	98	98
220	98	220	98	220	98	220	98
85	98	85	98	85	98	85	98
110	110	110	110	220	220	220	220
220	85	220	98	110	110	85	98

The moving spatial grid on the image is represented as

$$\left[\left((p-1) \frac{H}{P} + 1 \right), p \frac{H}{P} \right] \times \left[\left((q-1) \frac{W}{Q} + 1 \right), q \frac{W}{Q} \right].$$

The 2D-histograms are computed for the intensities present in the segments L_{s1} and L_{s2} . They are denoted as

$$h_{L_{s1}(i)} = \left\{ h_{L_{s1}(i)}(p, q) \mid 1 \leq p \leq P, 1 \leq q \leq Q \right\} \quad (8)$$

where the range of i is defined as $L_{\min} \leq i \leq L_{\text{med}} - 1$. $h_{L_{s1}}$ represents the 2D-histogram of the lower segment L_{s1} . Similarly, the 2D-histogram $h_{L_{s2}}$ for the upper segment L_{s2} is defined as

$$h_{L_{s2}(i)} = \left\{ h_{L_{s2}(i)}(p, q) \mid 1 \leq p \leq P, 1 \leq q \leq Q \right\} \quad (9)$$

where the range of i is defined as $L_{\text{med}} \leq i \leq L_{\max}$.

To visualize the 2D histogram, a sample image is considered and its 2D histogram is calculated using the equations from (5) to (7). Table 1 shows intensity values of the sample image I .

1. The number of distinct intensities present in the above example are 4. The median value for the above data is 104. Then lower histogram contains the intensities 85 and 98. They are lesser than the median value. The upper histogram contains the intensity values 110 and 220. They are greater than the median value.
2. According to the sample image the size of spatial grid is calculated using the following computations.

- $H = 8, W = 8$ and $l = 4$ for the Sample image I .
- $a_r = \frac{8}{8} = 1$.
- $P = \lfloor (4 \times 1)^{0.5} \rfloor = 2$, and $Q = \left\lfloor \left(\frac{4}{1} \right)^{0.5} \right\rfloor = 2$
- Size of the spatial grid is represented by $\frac{8}{2} \times \frac{8}{2}$. Based on the above calculation the sample image is divided into 4×4 spatial grids

The spatial grids are shown in Fig. 1 For the intensity 85 the 2D histogram based on the spatial grid is given below

$$h_{85} = \begin{bmatrix} 5 & 5 \\ 3 & 3 \end{bmatrix} \quad (10)$$

Similarly, the 2D histogram for the remaining intensities are calculated to obtain the discrete values using Rényi entropy and it is shown in Fig. 3 (see Fig. 2).

3.3. Detail extraction using Rényi entropy

Rényi entropy of the 2D-histogram is computed to incorporate the structural information in the formulation of discrete function.

$$\hat{r}_{L_{s1}}(i) = \frac{1}{1-\alpha} \log_2 \left(\sum_{p=1}^P \sum_{q=1}^Q \left(h_{L_{s1}(i)}(p, q) \right)^\alpha \right) \quad (11)$$

where $L_{\min} \leq i \leq L_{\text{med}} - 1$.

$$\hat{r}_{L_{s2}}(i) = \frac{1}{1-\alpha} \log_2 \left(\sum_{p=1}^P \sum_{q=1}^Q \left(h_{L_{s2}(i)}(p, q) \right)^\alpha \right) \quad (12)$$

where $L_{\text{med}} \leq i \leq L_{\max}$. $\hat{r}_{L_{s1}}$ and $\hat{r}_{L_{s2}}$ denote the Rényi entropies of the lower and upper segments, respectively. α controls the power of probability and it is chosen as '2' in this work. From the Rényi entropies the discrete functions are formulated as

$$\hat{f}_{L_{s1}}(i) = \frac{\hat{r}_{L_{s1}}(i)}{\sum_{x=L_{\min}}^{L_{\text{med}}-1} \hat{r}_{L_{s1}}(x) \text{ for } x \neq i} \quad (13)$$

$$\hat{f}_{L_{s2}}(i) = \frac{\hat{r}_{L_{s2}}(i)}{\sum_{x=L_{\text{med}}}^{L_{\max}} \hat{r}_{L_{s2}}(x) \text{ for } x \neq i} \quad (14)$$

3.4. Histogram clipping and equalization

Adaptive clipping limit is applied on the discrete function to control the enhancement rate. It is obtained by considering the minimum values among the mean, median and discrete value of each intensities in the segments. The following equations represent the clipped or modified discrete functions $\hat{f}_{L_{s1}\text{new}}$ and $\hat{f}_{L_{s2}\text{new}}$ for lower and upper segments, respectively.

$$\hat{f}_{L_{s1}\text{new}}(i) = \min[\hat{f}_{L_{s1}}(i), \text{mean}(\hat{f}_{L_{s1}}), \text{median}(\hat{f}_{L_{s1}})] \quad (15)$$

where $i = L_{\min}, L_{\min} + 1, \dots, L_{\text{med}} - 1$.

$$\hat{f}_{L_{s2}\text{new}}(i) = \min[\hat{f}_{L_{s2}}(i), \text{mean}(\hat{f}_{L_{s2}}), \text{median}(\hat{f}_{L_{s2}})] \quad (16)$$

where $i = L_{\text{med}}, L_{\text{med}} + 1, \dots, L_{\max}$. The modified discrete functions are normalized to compute the density functions.

$$\tilde{f}_{L_{s1}}(i) = \frac{\hat{f}_{L_{s1}\text{new}}(i)}{\sum_{x=L_{\min}}^{L_{\text{med}}-1} \hat{f}_{L_{s1}\text{new}}(x)} \quad (17)$$

$$\tilde{f}_{L_{s2}}(i) = \frac{\hat{f}_{L_{s2}\text{new}}(i)}{\sum_{x=L_{\text{med}}}^{L_{\max}} \hat{f}_{L_{s2}\text{new}}(x)} \quad (18)$$

The density functions are used to obtain the cumulative distribution functions (CDFs). The density functions for the lower histogram and upper histograms are denoted by $\tilde{f}_{L_{s1}}$ and $\tilde{f}_{L_{s2}}$ respectively. The CDFs are represented for lower and upper segments are $\tilde{F}_{L_{s1}}$ and $\tilde{F}_{L_{s2}}$ respectively. The CDF of the i^{th} intensity is calculated by adding the density functions of intensities from L_{\min} to the intensity i in the lower and upper segment from L_{med} to i .

$$\tilde{F}_{L_{s1}}(i) = \sum_{x=L_{\min}}^i \tilde{f}_{L_{s1}}(x) \quad (19)$$

where $i = L_{\min}, L_{\min} + 1, \dots, L_{\text{med}} - 1$.

$$\tilde{F}_{L_{s2}}(i) = \sum_{x=L_{\text{med}}}^i \tilde{f}_{L_{s2}}(x) \quad (20)$$

where $i = L_{\text{med}}, L_{\text{med}} + 1, \dots, L_{\max}$. From the CDF, the mapping function is enumerated and it is defined as,

$$\hat{I}(i) = \begin{cases} L_0 + (L_{\text{med}} - 1 + L_0) \times \tilde{F}_{L_{s1}}(i), & \text{for } L_{\min} \leq i \leq L_{\text{med}} - 1 \\ L_{\text{med}} + (L - L_{\text{med}}) \times \tilde{F}_{L_{s2}}(i), & \text{for } L_{\text{med}} \leq i \leq L_{\max} \end{cases} \quad (21)$$

where \hat{I} represents the equalized image. To enhance the image further, Discrete cosine transformation (DCT) is applied to the equalized image \hat{I} .

3.5. Local enhancement

The DCT coefficients of the image \hat{I} is altered by multiplying the weighting function $\hat{w}(m, n)$ to enhance the local regions of the image.

$$C(m, n) = c_m c_n \sum_{k=0}^{H-1} \sum_{l=0}^{W-1} \hat{I}(k, l) \cos \left(\frac{\pi(2k+1)m}{2 \times H} \right) \cos \left(\frac{\pi(2l+1)n}{2 \times W} \right) \quad (22)$$

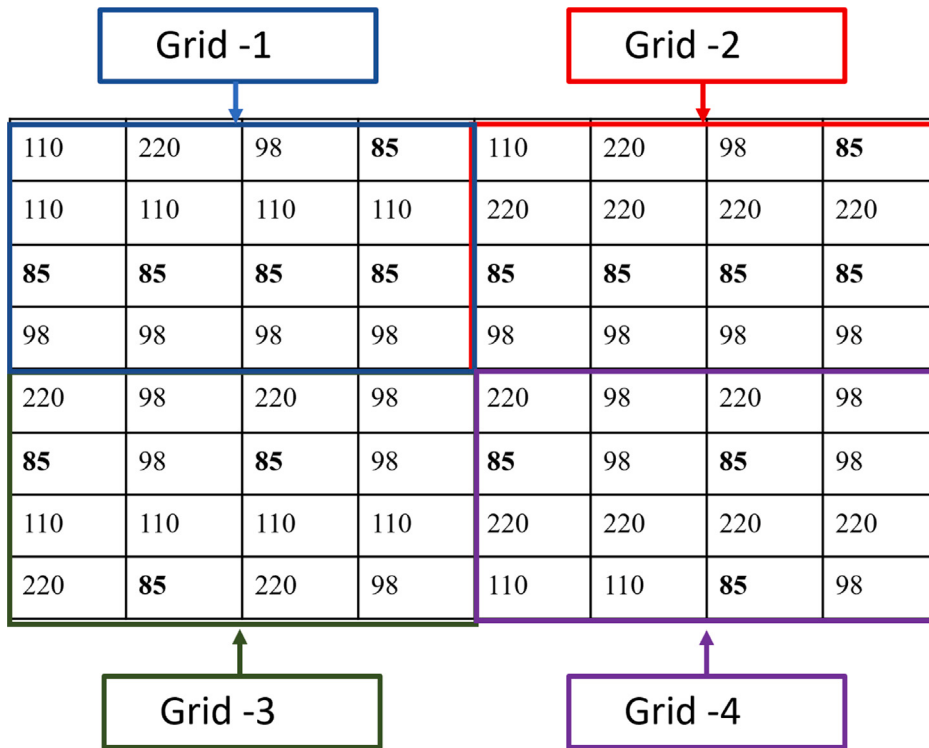


Fig. 2. Spatial grid for calculation of 2D-histogram.

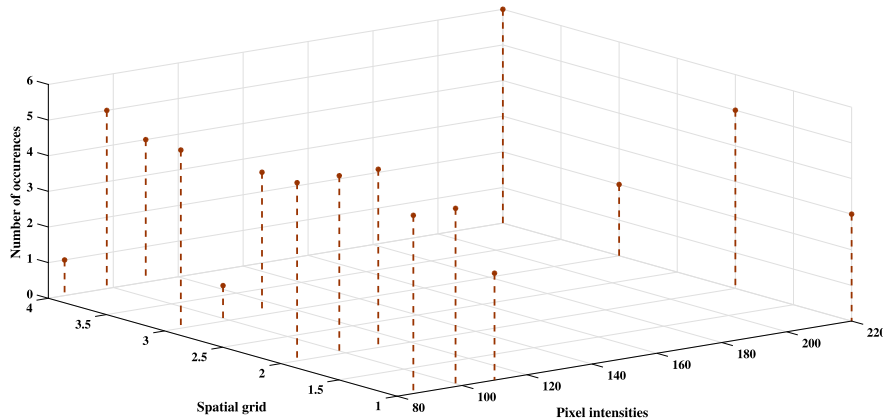


Fig. 3. 2D histogram of the example image.

where m and n vary from 0 to $(H - 1)$ and 0 to $(W - 1)$ respectively. $\hat{w}(m, n)$ is computed by

$$\hat{w}(m, n) = \left(1 + \frac{\rho - 1}{H - 1} \times m\right) \left(1 + \frac{\rho - 1}{W - 1} \times n\right) \quad (23)$$

where $\rho \geq 1$. To get higher enhancement, the value of ρ should be high. For the automatic selection of ρ , it is estimated from the normalized density function.

$$\rho = \left(\sum_{i=L_{\min}}^{L_{\max}} \tilde{f}_i \log_2(\tilde{f}_i) \right)^v \quad (24)$$

where $0 \leq v \leq 1$. The DCT coefficients are modified by the weighting function and it is represented as

$$C_{\text{mod}}(m, n) = C(m, n) \hat{w}(m, n) \quad (25)$$

Inverse DCT (IDCT) of the modified image results in a overall enhanced image \hat{I}_{en} .

$$\hat{I}_{en}(k, l) = \sum_{m=0}^{H-1} \sum_{n=0}^{N-1} c_m c_n C_{\text{mod}}(m, n) \cos\left(\frac{\pi(2k+1)m}{2 \times H}\right) \cos\left(\frac{\pi(2l+1)n}{2 \times W}\right) \quad (26)$$

4. Experimental results

The performance of the suggested algorithm is demonstrated with the experimental results obtained by testing the technique on four databases namely TID2013 [47,48], CSIQ [49], LOL [50], and CEED [51]. These databases are considered due to the homogeneous background images. A number of existing low light image enhancement methods are considered for comparison to validate the efficiency of the

Table 2
Specifications of the test images.

Images	Database	Size
img11 (SI1)	CEED	512×512
img16 (SI2)	CEED	512×512
img19 (SI3)	CEED	512×512
img24 (SI4)	CEED	512×512
cactus.contrast.5 (SI5)	CSIQ	512×512
swarm.contrast.5 (SI6)	LOL	512×512
129 (SI7)	LOL	600×400
i16 (SI8)	TID2013	512×384
i20 (SI9)	TID2013	512×384
i21 (SI10)	TID2013	512×384

proposed method. Edge enhancing bi-histogram equalization (EEBHE) [24] (2019), and joint histogram equalization (JHE) [29] (2019) from histogram based approaches, LIME [33] (2017) and STRU [34] (2018) from illumination enhancement methods, LLnet [40] (2018), MIRnet [42] (2020) and EGAN [41] from convolutional neural network (CNN) are considered for comparison.

Although the techniques are evaluated on complete datasets, sample images from the aforementioned databases have been used to describe the subjective and numerical evaluations. The database and the size of the considered samples are detailed in [Table 2](#).

4.1. Databases

This section provides the detail about databases used in this research work. They are namely categorical subjective image quality (CSIQ) [49] database, Tampere image database (TID2013) [47], low light dataset (LOL) [50], and CEED [51] database. Images are distorted in CSIQ database using one of six different forms of distortions at four to five different degrees. The six distinct distortions are achieved through the use of additive pink Gaussian noise, Gaussian blurring, global contrast decrements, and JPEG compression. This database is more beneficial when original data is required to evaluate the algorithm's performance. It contains 30 undistorted images with a resolution of 512×512 .

TID2013 is a database aimed at evaluating full-reference visual quality assessment criteria. The database comprises a greater number of test images (3000), which were generated from 25 reference photos, 24 types of distortions for each reference image, and 5 levels for each type of distortion. The database has the images of size 512×384 .

LOL database is developed for the purpose of designing a deep learning model for contrast enhancement. It consists of 500 low contrast (distorted) and high contrast (reference) images with the size of 600×400 . The low contrast images are generated by limiting the exposure time during image acquisition and CEED has 30 low light images.

4.2. Qualitative analysis

[Fig. 4](#) to [Fig. 7](#) show the sample and the enhanced images obtained from the representative algorithms and the proposed method along with their respective histograms considered from CEED database. [Fig. 4\(a\)](#) is a homogeneous background image and most of the pixels have similar intensities. This causes histogram peaks and produces halo artifacts in the processed images. It can be visualized from its respective histogram which is shown in [Fig. 4\(e\)](#). [Fig. 4\(b\)](#) depicts an enhanced image resulted from EEBHE technique. It does not alter the dynamic gray scale range of the input image during the equalization process and transforms the intensities with in the same range. So, the resultant image from EEBHE has less improvement in the visual appearance. [Fig. 4\(c\)](#) depicts the enhanced image from JHE technique. Due to the employment of the average spatial information in the equalization process, it results in smoothed edges of the grass in the background

of the image. The enhanced image obtained from LIME is displayed in [Fig. 4\(d\)](#). It is observed from the figure that the overall luminance of the image is improved which produces a bright image compared to the input. [Fig. 4\(i\)](#) shows an enhanced image obtained from the STRU method. The resultant image looks bright though its background gets smoothed. [Fig. 4\(j\), \(k\) and \(l\)](#) depict the resultant images from LLnet, MIRnet and EGAN, respectively. The overall brightness of the processed images is improved but the discrimination between various regions are minimum in the enhanced images and the images also suffer from over enhancement.

[Fig. 4\(q\)](#) displays the improved image obtained from the suggested Rényi entropy based algorithm. It is observed from the figure that, the visual appearance of the image has improved without color distortion and various elements of the scene are seen clearly in the illustration. This may be because the proposed technique makes extensive use of dynamic gray scale and it can be visualized from the respective histogram shown in [Fig. 4\(r\)](#).

[Fig. 5\(a\)](#) shows a degraded image with uneven distribution of gray values. Due to the improper utilization of dynamic gray scale EEBHE results in the improved image similar to the input which can be seen in [Fig. 5\(b\)](#). The processed image obtained from the JHE technique is shown in [Fig. 5\(c\)](#) where the background is distorted and the foreground information is visible due to the averaging process employed. [Fig. 5\(d\), \(i\), \(j\) and \(l\)](#) show the improved images obtained from LIME, STRU, LLnet, and EGAN, respectively. It is noticed from the figure that the foggy appearance of the results decrease the visualization of the image information. The resultant image obtained from MIRnet is shown in [Fig. 5\(k\)](#) where the edges of the berries are affected by halo artifacts. [Fig. 5\(q\)](#) displays the output image from the proposed method. Here, the background information is more prominent along with clear distinction of the berries in the foreground. The similar effect can be seen in [Figs. 6](#) and [7](#).

[Fig. 8](#) exhibits the output images obtained from the various enhancement techniques for the test image which belongs to CSIQ database. The Figure includes the ground truth information as reference image for the comparative analysis of the enhancement techniques. [Fig. 8\(b\)](#) shows the input image. Due to the poor dynamic range, it is difficult to discriminate the various regions in the image. [Fig. 8\(c\)](#) depicts the resultant image from EEBHE technique and it looks similar to the input because of the limited utilization of the dynamic gray scale after the transformation. JHE produces an image with high contrast but it over-enhances few regions results in washed out appearance. The artifact can be seen near the bird and the flower region of the image. [Fig. 8\(i\)](#) to [Fig. 8\(l\)](#) and [Fig. 8\(q\)](#) images are produced by the retinex and deep learning based approaches, respectively. Though, the color information is enhanced but the foggy appearance of the improved images hide the discrimination between the objects. [Fig. 8\(s\)](#) displays the enhanced image produced by the proposed method. The image and its histogram are similar to the reference image and its histogram. The color information is enhanced and the foggy appearance is also removed from the enhanced image.

In [Fig. 9](#), the input image has fewer number of distinct intensities, rendering the scene's objects nearly unnoticeable. The output images obtained due to enhancement have minor improvement in their contrast, which is noticed in [Fig. 9\(c\), \(d\), \(i\), \(j\), \(k\), \(l\)](#) and [\(q\)](#) produced by EEBHE, JHE, LIME, STRU, LLnet, MIRnet, and EGAN algorithms, respectively. Due to fewer number of intensities after the enhancement and failed to disperse the intensities in the complete dynamic gray scale the objects in the resultant images are not visible with clear discrimination.

[Fig. 9\(s\)](#) produces the enhanced images with clear discrimination between the objects by the proposed method. This image is enhanced with good color details in comparison with the high contrast reference image of the database. Further, it is inferred that the proposed method results in enhanced images from concealed details of the images.

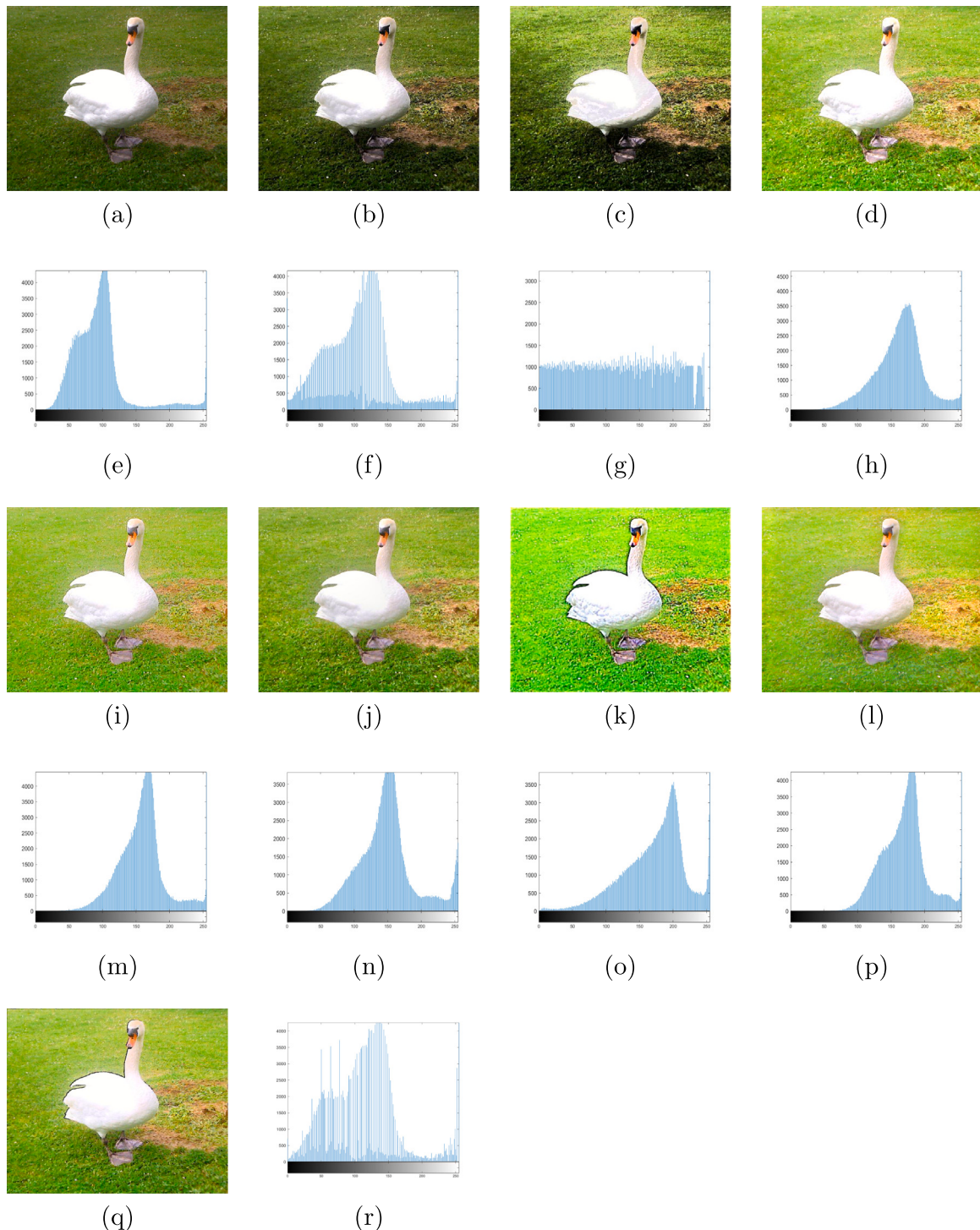


Fig. 4. Contrast enhancement results of SII: (a) input, (b) EEBHE, (c) JHE, (d) LIME, (e) histogram of input, (f) histogram of EEBHE, (g) histogram of JHE, (h) histogram of LIME, (i) STRU, (j) LLnet, (k) MIRnet, (l) EGAN, (m) histogram of STRU, (n) histogram of LLnet, (o) histogram of MIRnet, (p) histogram of EGAN, (q) proposed method, and (r) histogram of proposed method.

Fig. 10 displays the low contrast input and processed output images produced by the representative methods along with the proposed method from the LOL database. The majority of the database's dark photographs were captured indoors, while only a few were captured outdoors. **Fig. 10(c)** shows the resultant image obtained from EEBHE. Though the visual appearance of the image is improved however, the distinct regions in the image are not distinguishable. **Fig. 10(d)** depicts the enhanced result achieved via JHE, in which the features are recognizable but the processed images lack color information. **Fig. 10(i), (j),**

(k), (l) and (q) show the upgraded images obtained by LIME, STRU, LLnet, MIRnet, and EGAN. Unlike histogram equalization methods, illumination correction based approaches and neural network architectures yield significantly more contrast-enhanced images. However, the object's edges require improvement.

Fig. 10(s) depicts the processed images derived from the proposed method, in which it is easy to distinguish between the numerous items in the image's foreground and background as a result of the substantial contrast enhancement in the processed image.

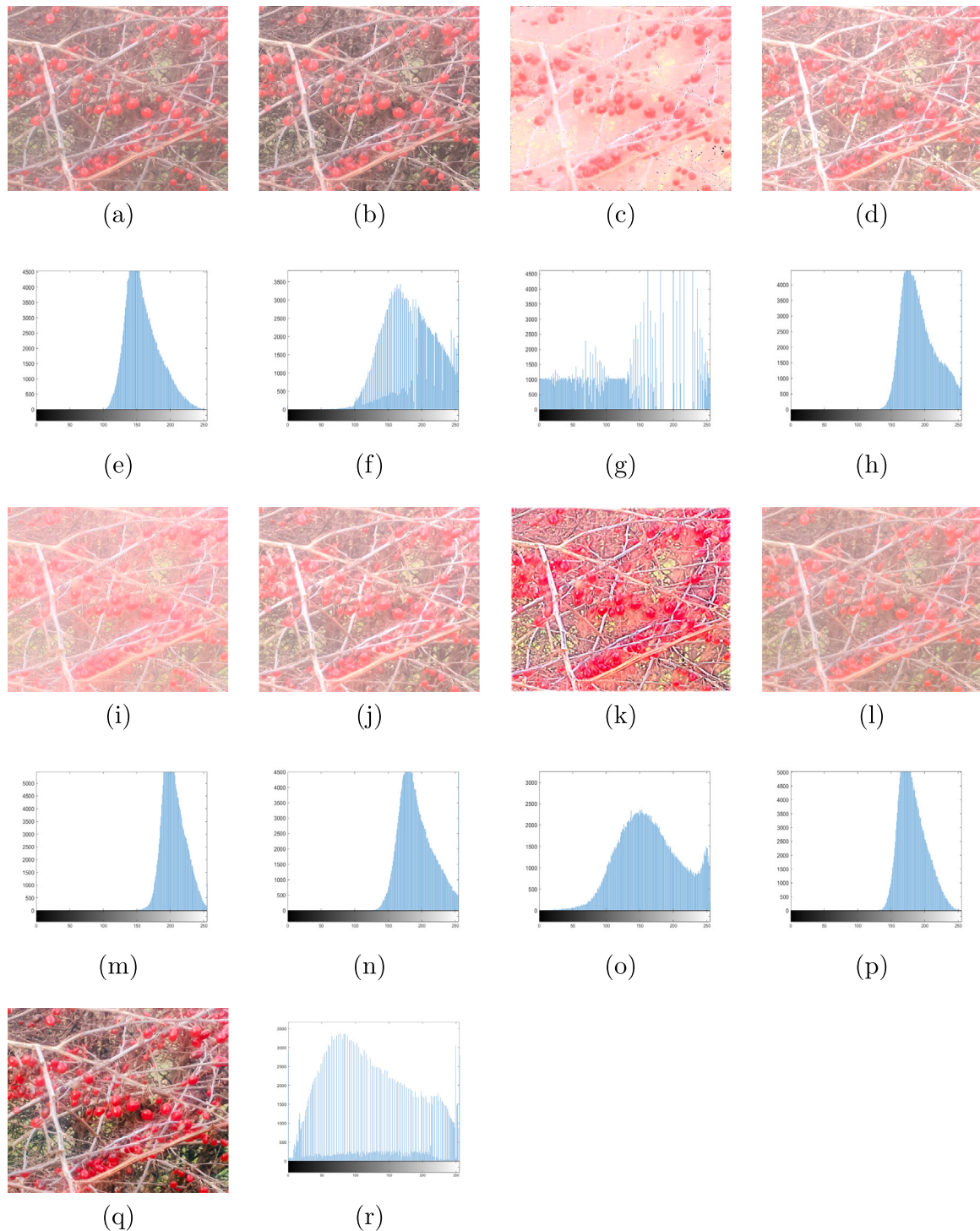


Fig. 5. Contrast enhancement results of SI2: (a) input, (b) EEBHE, (c) JHE, (d) LIME, (e) histogram of input, (f) histogram of EEBHE, (g) histogram of JHE, (h) histogram of LIME, (i) STRU, (j) LLnet, (k) MIRnet, (l) EGAN, (m) histogram of STRU, (n) histogram of LLnet, (o) histogram of MIRnet, (p) histogram of EGAN, (q) proposed method, and (r) histogram of proposed method.

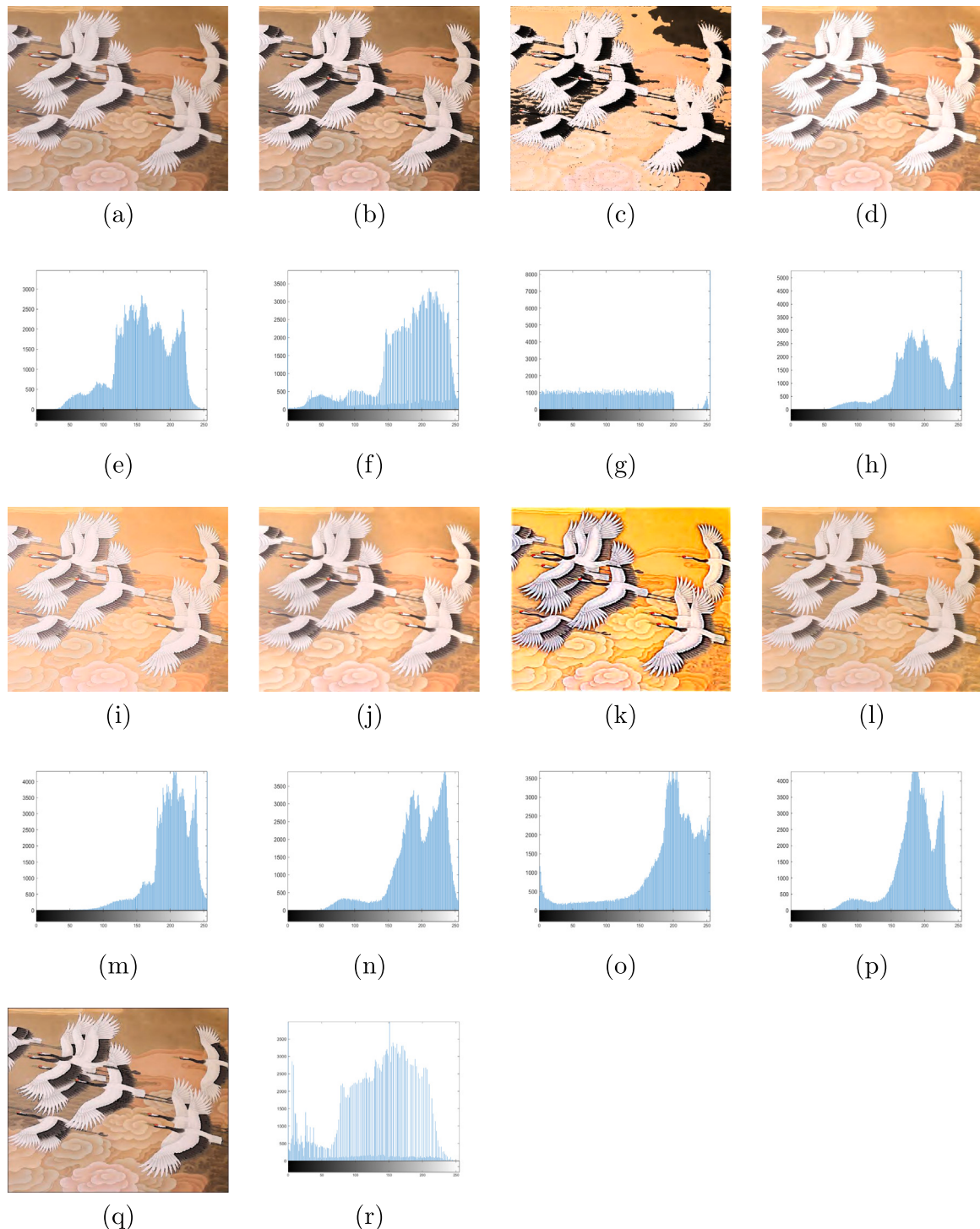


Fig. 6. Contrast enhancement results of SI3: (a) input, (b) EEBHE, (c) JHE, (d) LIME, (e) histogram of input, (f) histogram of EEBHE, (g) histogram of JHE, (h) histogram of LIME, (i) STRU, (j) LLnet, (k) MIRnet, (l) EGAN, (m) histogram of STRU, (n) histogram of LLnet, (o) histogram of MIRnet, (p) histogram of EGAN, (q) proposed method, and (r) histogram of proposed method.

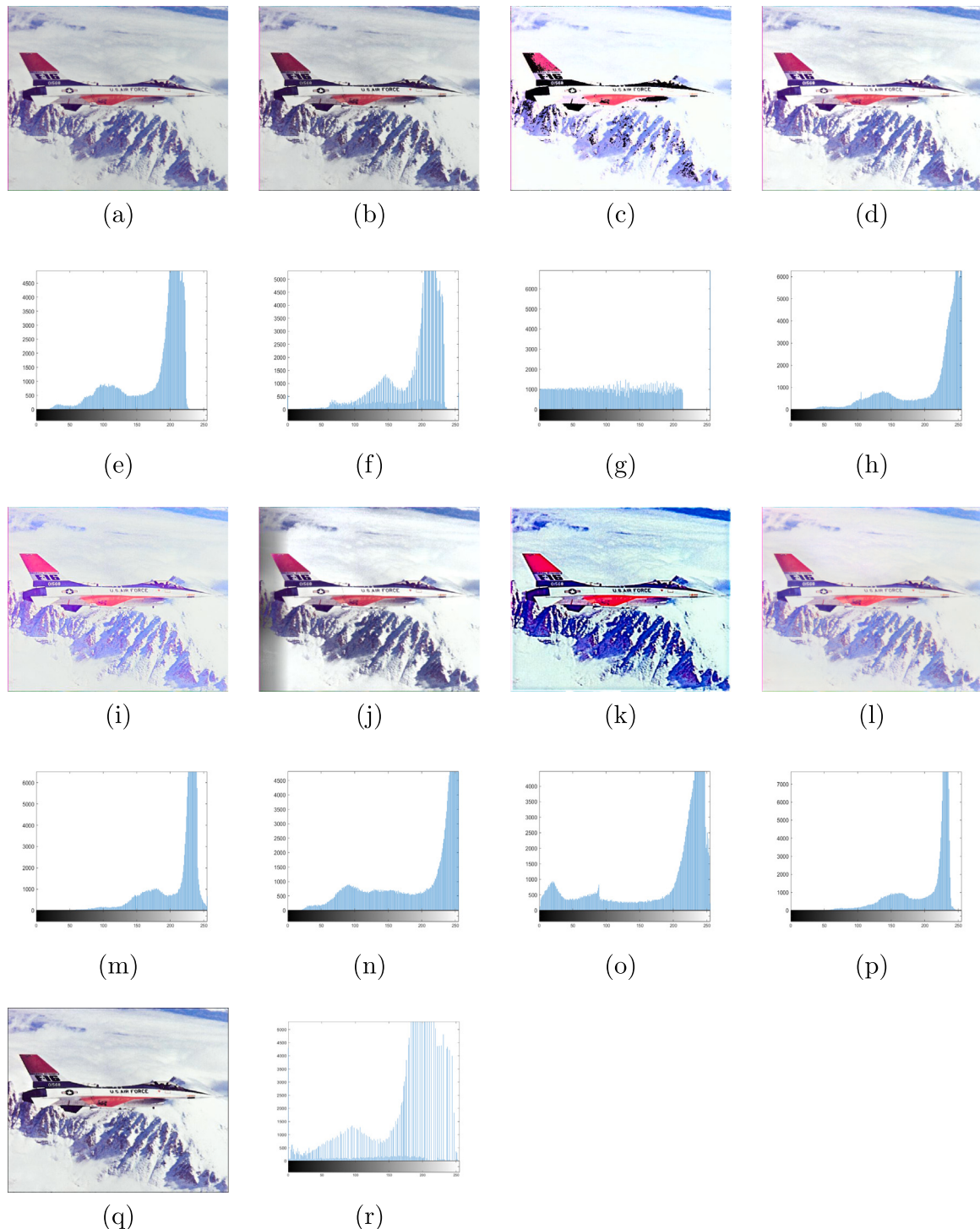


Fig. 7. Contrast enhancement results of SI4: (a) input, (b) EEBHE, (c) JHE, (d) LIME, (e) histogram of input, (f) histogram of EEBHE, (g) histogram of JHE, (h) histogram of LIME, (i) STRU, (j) LLnet, (k) MIRnet, (l) EGAN, (m) histogram of STRU, (n) histogram of LLnet, (o) histogram of MIRnet, (p) histogram of EGAN, (q) proposed method, and (r) histogram of proposed method.

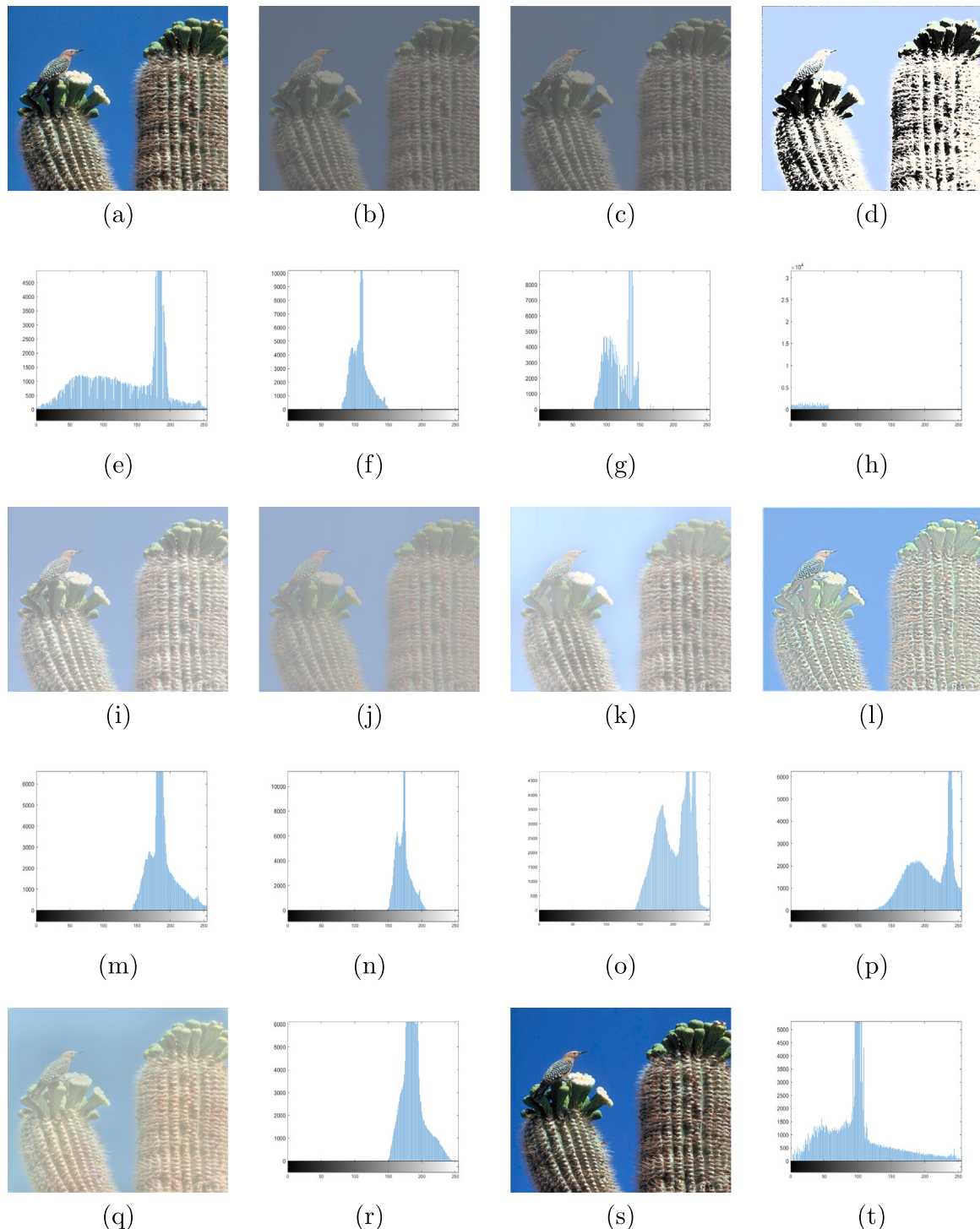


Fig. 8. Contrast enhancement results of SI5: (a) reference (b) input, (c) EEBHE, (d) JHE, (e) histogram of reference, (f) histogram of input, (g) histogram of EEBHE, (h) histogram of JHE, (i) LIME, (j) STRU, (k) LLnet, (l) MIRnet, (m) histogram of LIME, (n) histogram of STRU, (o) histogram of LLnet, (p) histogram of MIRnet, (q) EGAN, (r) histogram of EGAN, (s) proposed method, and (t) histogram of proposed method.

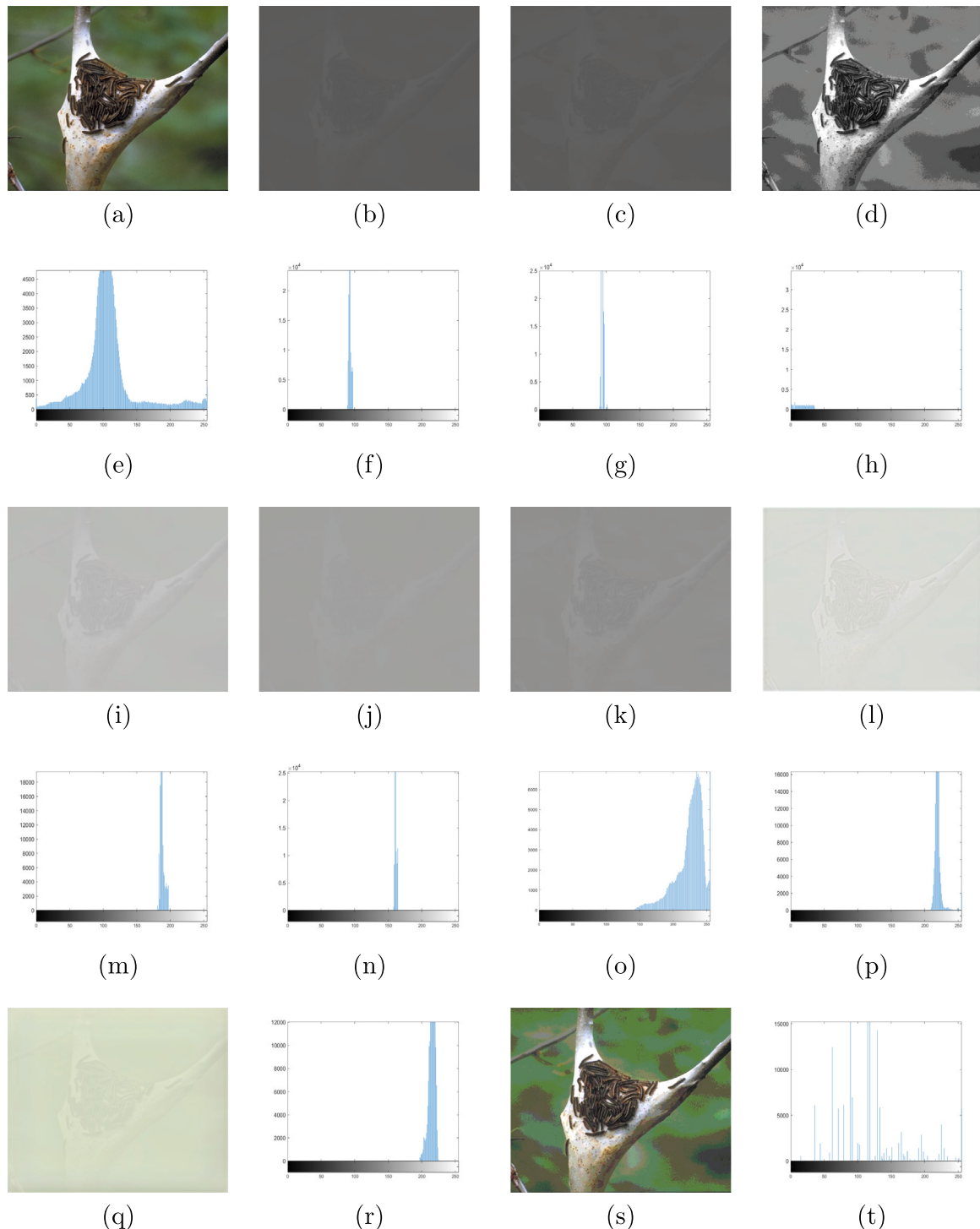


Fig. 9. Contrast enhancement results of SI6: (a) reference (b) input, (c) EEBHE, (d) JHE, (e) histogram of reference, (f) histogram of input, (g) histogram of EEBHE, (h) histogram of JHE, (i) LIME, (j) STRU, (k) LLnet, (l) MIRnet, (m) histogram of LIME, (n) histogram of STRU, (o) histogram of LLnet, (p) histogram of MIRnet, (q) EGAN, (r) histogram of EGAN, (s) proposed method, and (t) histogram of proposed method.

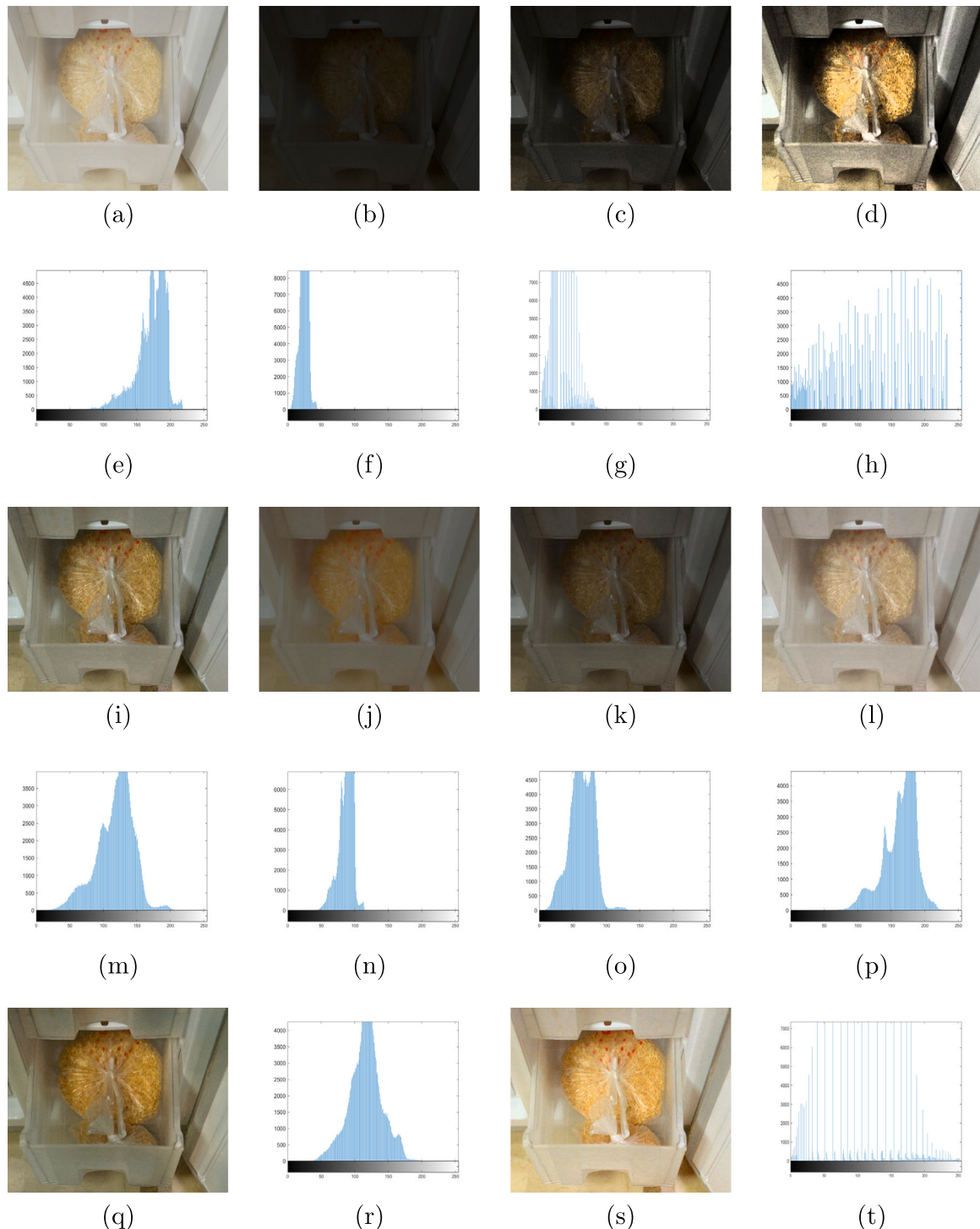


Fig. 10. Contrast enhancement results of SI7: (a) reference (b) input, (c) EEBHE, (d) JHE, (e) histogram of reference, (f) histogram of input, (g) histogram of EEBHE, (h) histogram of JHE, (i) LIME, (j) STRU, (k) LLnet, (l) MIRnet, (m) histogram of LIME, (n) histogram of STRU, (o) histogram of LLnet, (p) histogram of MIRnet, (q) EGAN, (r) histogram of proposed method and (t) histogram of proposed method.

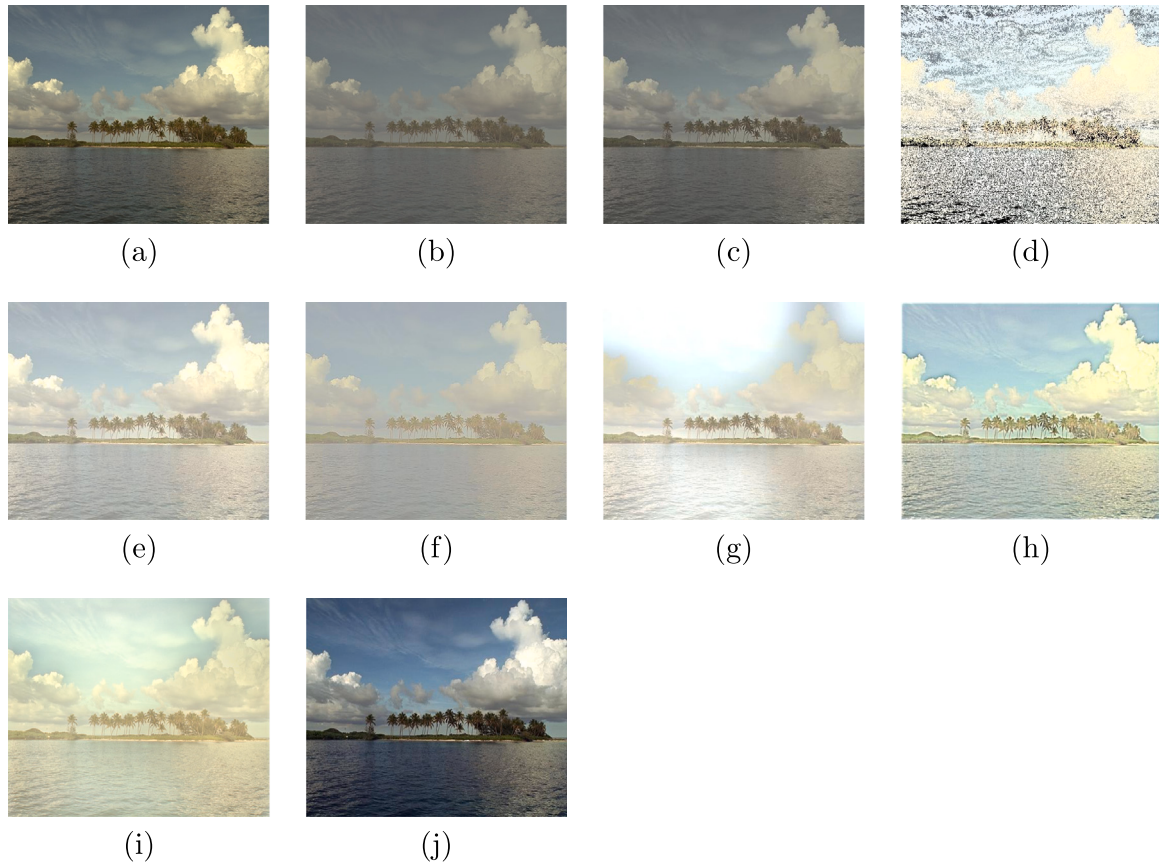


Fig. 11. Contrast enhancement results of SI8: (a) reference (b) input, (c) EEBHE, (d) JHE, (e) LIME, (f) STRU, (g) LLnet, (h) MIRnet, (i) EGAN, and (j) proposed method.

Figs. 11 to 13 depict the upgraded images obtained from the suggested approach and the existing approaches for the test images of TID2013 database. All the sample images have uniform background. The histogram spikes in the input images cause the artifacts in the processed images obtained by JHE technique and are represented in **Fig. 11(d)** to **Fig. 13(d)**. The retinex and deep learning based approaches produce the images those are displayed in **Fig. 11(e)–(i)** to **Fig. 13(e)–(i)**. The improved images have no artifacts but the amount of perceived contrast is less in the resultant pictures. It is noticed from **Fig. 11(j)** to **Fig. 13(j)** that the suggested method produces a enhanced images that look like the reference images without artifacts and increment in the visibility of the processed images.

From the visual interpretation, it is clear that the proposed method improves input pictures of various sorts, such as those with a restricted dynamic range, a dark background, and a uniform background, with fewer or no artifacts in the resultant enhanced images.

4.3. Quantitative analysis

- Relative contrast enhancement (REC) [58] quantifies the contrast of the enhanced image. Higher values of REC indicate the better contrast improvement of the processed image.

$$REC = \frac{C(J)}{C(I)} \quad (27)$$

where $C(J) = 20 \times \log \left[\frac{1}{M \times N} \sum_{x=1}^M \sum_{y=1}^N J^2(x, y) - \left| \frac{1}{M \times N} \sum_{x=1}^M \sum_{y=1}^N J(x, y) \right|^2 \right]$ ‘I’ and ‘J’ are the input and the enhanced images respectively. ‘M’ and ‘N’ represent the number of rows and columns of the image. ‘x’ and ‘y’ are the spatial co-ordinates of the image.

- Contrast improvement factor (CIR) [59] quantifies the local contrast improvement. Higher values of CIR signify the better local contrast improvement in the enhanced image.

$$CIR(I, J) = \frac{\sum_{(x,y) \in D} |w(x, y) - \bar{w}(x, y)|^2}{\sum_{(x,y) \in D} w(x, y)^2} \quad (28)$$

‘w’and ‘ \bar{w} ’are the local contrast of the ‘I’and ‘J’respectively. ‘D’ denotes the region of size 3×3 . $w(x, y) = \frac{|\rho-i|}{|\rho+i|}$ where ‘ ρ ’ is the center pixel and ‘ i ’ is the mean of the neighboring pixel in ‘D’.

- Spatial frequency (SF) [60] measures the spatial information of the image. Large value of SF indicates the more spatial information of the processed image.

$$SF = \sqrt{CF^2 + RF^2} \quad (29)$$

where

$$CF = \sqrt{\frac{1}{M \times N} \sum_{x=1}^M \sum_{y=1}^N (J(x, y) - J(x, y-1))^2},$$

$$RF = \sqrt{\frac{1}{M \times N} \sum_{x=1}^M \sum_{y=1}^N (J(x, y) - J(x-1, y))^2}$$

The primary objective of the suggested approach is to produce a high contrast image while optimizing the information content and preserving image details with minimal or no visual artifacts. The quantitative metrics are chosen to validate the objectives of the proposed methodology. **Table 3** provides the details about the metrics for numerical analysis. Contrast improvement index (CII), standard deviation (SD), discrete entropy (DE), natural image quality evaluator (NIQE), peak signal to noise ratio (PSNR) [55], structural similarity index (SSIM), and average mean brightness

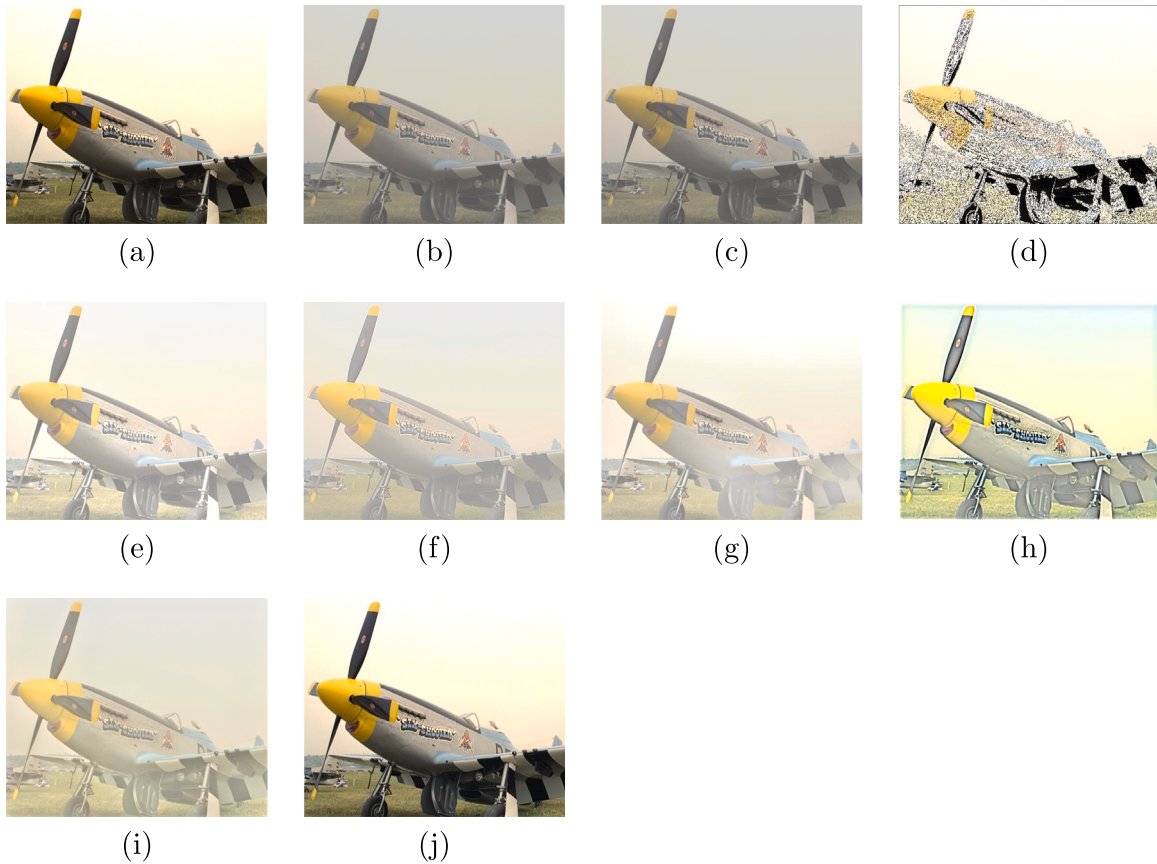


Fig. 12. Enhanced images of SI9: (a) reference (b) input, (c) EEBHE, (d) JHE, (e) LIME, (f) STRU, (g) LLnet, (h) MIRnet, (i) EGAN, and (j) proposed method.

Table 3
Various performance measures.

S.no	Measures	Mathematical representation	Highlights	Range
1	CII [52]	$CII = \frac{M(C_{loc}(J))}{M(C_{loc}(I))}$ $C_{loc} = \frac{\max - \min}{\max + \min}$ for a 3×3 window.	Local contrast improvement with respect to neighbors.	More than the input image.
2	SD [52]	$SD = \sqrt{\sum_{k=0}^{L-1} (J_k - M(J))^2 \times pdf(J_k)}$	Global contrast enhancement.	More than the input image.
3	DE [53]	$E(I) = -\sum_{i=1}^P p(i_j) \log_2 p(i_j)$	Amount of information loss.	Maximum value: 8 bits/symbol.
4	SSIM [54]	$SSIM(I, J) = \frac{(2\mu_I\mu_J + c_1)(2\sigma_{IJ} + c_2)}{(\mu_I^2 + \mu_J^2 + c_1)(\sigma_I^2 + \sigma_J^2 + c_2)}$ $c_1 = 6.5; c_2 = 58.5$	Degradation due to processing	0-1.
5	PSNR [55]	$PSNR = 10 \log_{10} \left[\frac{(L-1)^2}{\frac{1}{M \times N} \sum_{x,y} I(x,y) - J(x,y) ^2} \right]$	1. Reconstruction quality. 2. Amount of deviation between original and enhanced image.	Range: 30 - 50 dB for an 8-bit image
6	NIQE [56]	$NIQE = \sqrt{\left((v_1 - v_2)^T \left(\frac{\Sigma_1 + \Sigma_2}{2} \right)^{-1} (v_1 - v_2) \right)}$	Degradation due to processing	Low value indicates less distortion.
7	AMBE [57]	$AMBE = M(I) - M(J) $	1. Preservation of mean brightness. 2. Amount of mean shifting.	0 to any positive value within the dynamic range.

I =low contrast image, J =enhanced image, $M(\cdot)$ =mean, $E(\cdot)$ =entropy, v_1 and Σ_1 =mean vector and covariance matrix of natural multi-variate Gaussian model v_2 and Σ_2 =mean vector and covariance matrix of multi-variate Gaussian model of the enhanced image.

error (AMBE) are measured for the improved images produced from the existing methods and suggested algorithm for the quantitative analysis. The quantitative metrics for the test images are listed in the **Table 4** to **Table 10**. The optimal values for individual

metric are highlighted in bold. To increment the correctness of the evaluation, the approaches utilized in the literature in addition to the suggested technique are used for assessment on entire data base. The mean values of the quantitative metrics obtained from

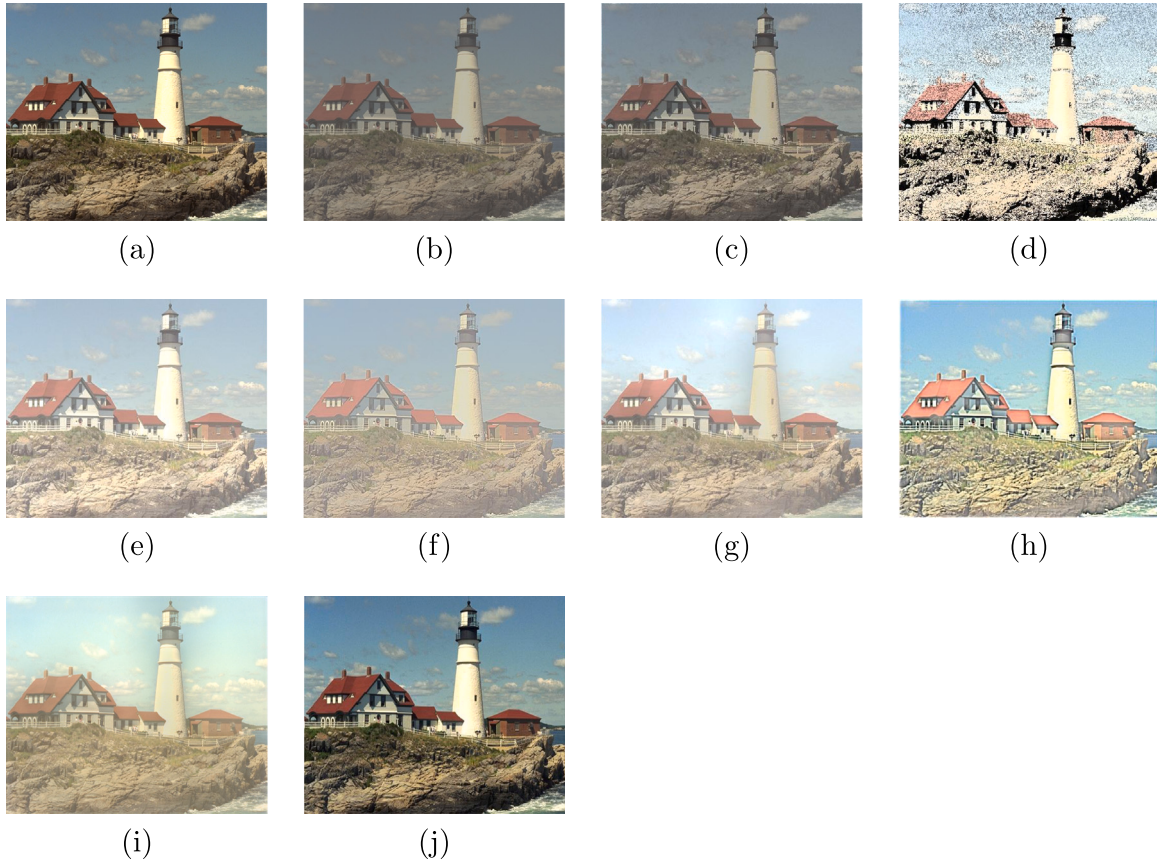


Fig. 13. Contrast enhancement results of SI10: (a)reference (b) input, (c) EEBHE, (d) JHE, (e) LIME, (f) STRU, (g) LLnet, (h) MIRnet, (i) EGAN, and (j) proposed method.

Table 4
PSNR results from different CE approaches for the test images.

Methods/ Images	EEBHE (2019)	JHE (2019)	LIME (2017)	STRU (2018)	LLnet (2018)	MIRnet (2020)	EGAN (2021)	Proposed
SI1	22.16	15.41	10.96	12.03	13.88	9.96	11.09	31.09
SI2	15.64	11.47	17.29	14.71	17.46	17.99	12.41	18.01
SI3	22.83	11.31	16.41	14.79	16.26	14.46	10.67	28.71
SI4	22.10	12.06	16.93	16.52	17.56	16.93	11.88	23.99
SI5	13.38	13.50	9.61	10.67	7.22	8.74	9.51	14.21
SI6	16.29	8.02	8.44	10.84	6.08	9.56	6.37	22.62
SI7	5.21	8.72	9.97	11.81	7.07	12.26	8.48	22.81
SI8	24.03	9.76	10.91	11.19	10.52	9.93	11.28	19.16
SI9	18.86	7.87	10.53	11.88	9.79	15.23	10.45	19.73
SI10	5.26	10.94	13.18	9.42	7.31	9.12	12.92	15.03

the suggested and the representative methods for the complete databases are displayed in Fig. 15.

PSNR values of the improved images produced from the different existing algorithms and the suggested technique are listed in the Table 4 to evaluate the restoration capability of the algorithms. It is observed from the values that the proposed method yields the high PSNR value compared to the other representative methods existing in the literature. It indicates that the employment of structural information in the proposed technique helps to enhance the regions based on its nature and it produces the improved image with minimum error in comparison with the ground truth information.

Table 5 lists the SSIM values of the sample images considered from the four databases. SSIM is used to measure the loss of structural information after processing. The suggested algorithm results in high

SSIM value except SI2 for all the sample images in comparison with the existing methods. It shows that the incorporation of the structural information leads to preservation of edge detail in the processed images.

Table 6 details the CII values produced from test pictures using the various methodologies stated in the literature, and the suggested technique. CII identifies an increment in contrast in the neighborhood. From the table it is observed that, the proposed method surpasses the existing algorithms with respect to CII value for the databases used for analysis. The CII values provided by EEBHE and JHE are comparable to those obtained with the proposed approach. Using LIME, STRU, and the neural network architectures LLnet, MIRnet, and EGAN may result in an increase in average luminance and a minor enhancement in local areas, as indicated by the minimum CII value of the sample pictures analyzed in the investigation. Due to the presence of structural information in

Table 5
SSIM results from different CE approaches for the test images.

Methods/ Images	EEBHE (2019)	JHE (2019)	LIME (2017)	STRU (2018)	LLnet (2018)	MIRnet (2020)	EGAN (2021)	Proposed
SI1	0.94	0.61	0.72	0.83	0.83	0.57	0.84	0.97
SI2	0.84	0.33	0.92	0.91	0.92	0.64	0.8	0.93
SI3	0.93	0.5	0.95	0.89	0.95	0.72	0.81	0.98
SI4	0.95	0.6	0.96	0.91	0.94	0.73	0.73	0.97
SI5	0.70	0.45	0.7	0.58	0.68	0.56	0.67	0.87
SI6	0.71	0.46	0.58	0.61	0.52	0.24	0.53	0.76
SI7	0.26	0.23	0.71	0.73	0.56	0.24	0.75	0.75
SI8	0.92	0.53	0.83	0.80	0.73	0.18	0.78	0.93
SI9	0.85	0.21	0.82	0.78	0.79	0.36	0.80	0.91
SI10	0.28	0.20	0.81	0.82	0.78	0.20	0.79	0.92

Table 6
CII results from different CE approaches for the test images.

Methods/ Images	EEBHE (2019)	JHE (2019)	LIME (2017)	STRU (2018)	LLnet (2018)	MIRnet (2020)	EGAN (2021)	Proposed
SI1	1.08	1.28	0.97	0.95	0.92	1.26	0.72	1.31
SI2	1.49	0.46	0.93	0.77	0.91	2.01	0.73	2.32
SI3	1.03	1.44	0.90	0.96	0.85	2.31	0.56	2.32
SI4	1.57	1.84	0.95	0.83	1.10	2.53	0.73	2.60
SI5	1.11	3.78	0.99	0.68	0.41	0.65	1.06	4.08
SI6	1.14	1.18	0.99	0.84	0.89	0.56	1.06	4.51
SI7	1.17	1.23	0.99	0.78	0.56	1.03	0.56	1.62
SI8	1.29	1.75	0.97	0.79	0.89	1.36	0.83	3.102
SI9	1.03	2.52	0.92	0.79	0.78	1.36	0.82	2.61
SI10	1.35	2.41	0.95	0.96	0.84	0.90	0.79	2.64

Table 7
SD results from different CE approaches for the test images.

Methods/ Images	EEBHE (2019)	JHE (2019)	LIME (2017)	STRU (2018)	LLnet (2018)	MIRnet (2020)	EGAN (2021)	Proposed
SI1	50.5	52.02	42.03	38.5	41.5	47.3	24.3	53.95
SI2	39.09	15.63	26.67	17.02	25.98	45.14	45.72	46.71
SI3	45.81	51.03	42.35	31.68	39.23	47.19	35.48	51.12
SI4	41.54	54.4	51.03	34.25	63.24	75.85	54.33	56.52
SI5	17.97	34.21	19.15	9.18	24.40	30.96	16.07	44.01
SI6	17.8	15.2	12.26	12.23	13.25	14.68	14.18	41.04
SI7	17.35	42.12	27.81	14.7	17.96	24.31	22.12	40.9
SI8	25.71	42.12	23.15	26.6	25.43	61.20	26.42	49.48
SI9	43.63	62.13	33.07	220.42	30.52	46.15	40.75	73.7
SI10	30.87	50.16	29.77	23.36	36.77	51.65	24.08	51.36

Table 8
AMBE results from different CE approaches for the test images.

Methods/ Images	EEBHE (2019)	JHE (2019)	LIME (2017)	STRU (2018)	LLnet (2018)	MIRnet (2020)	EGAN (2021)	Proposed
SI1	6.84	14.76	68.5	61.05	48.20	73.84	70.64	5.05
SI2	25.25	62.3	33.9	45.79	48.34	24.25	53.37	22.36
SI3	11.81	15.64	37.99	43.89	36.69	28.8	71.03	9.3
SI4	17.2	47.7	35.61	34.83	35.26	28.3	59.40	12.27
SI5	36.3	65.4	78.11	63.99	69.3	89.3	77.6	10.26
SI6	12.4	61.3	85.19	68.27	89.3	92.3	96.3	21.09
SI7	16.7	85.5	89.01	61.5	38.7	139.2	92.42	25.63
SI8	13.6	34.3	80.23	38.7	58.9	101.9	33.69	10.3
SI9	6.47	68.8	48.26	59.84	49.8	24.24	71.5	5.94
SI10	7.18	62.3	74.28	62.77	78.9	52.9	91.25	4.1

the equalization process, the proposed strategy increases the contrast in local areas, possibly producing a high CII value for all sample images in comparison with various methods used in literature.

SD values obtained for the sample images are displayed in Table 7. The dispersion of pixel values in the entire gray scale produces an image with significant contrast. SD measures the dispersion of intensities. From the table it is observed that, the suggested method yields a larger SD for the test pictures with the exception of SI7 and SI8. Table 7 reveals that LIME, STRU, LLnet, MIRnet and EGAN mimic the dispersion of the input image which might result in substantial enhancement in the global contrast. The proposed method considers

detail information by adjusting intensities and produces an improved image encompassing the whole dynamic range. It enables the proposed technique to attain a higher SD value in comparison to representative algorithms existing in the literature.

Table 8 show the AMBE values of sample images from the four databases. The maintenance of mean luminance aids in the minimization of display device-induced artifacts, as indicated by the low AMBE. Table 8 indicate that the EEBHE approach generate the low AMBE values. Inefficient utilization of entire gray scale, as demonstrated by their low CII and SD values, prevent them from fulfilling their primary objective of enhancing contrast. JHE, LIME, STRU, LLnet, MIRnet and

Table 9
DE results from different CE approaches for the test images.

Methods/ Images	Input	EEBHE (2019)	JHE (2019)	LIME (2017)	STRU (2018)	LLnet (2018)	MIRnet (2020)	EGAN (2021)	Proposed
SI1	6.88	7.07	7.12	6.72	7.19	7.09	7.03	5.94	7.13
SI2	6.59	7.04	6.80	6.58	6.57	6.57	7.45	7.07	7.55
SI3	7.31	7.18	7.09	6.88	7.04	7.04	7.3	6.91	7.57
SI4	6.70	6.50	6.31	6.45	6.78	6.99	7.07	7.05	7.15
SI5	5.02	5.32	2.12	5.94	6.12	6.38	6.29	5.89	6.92
SI6	2.07	1.74	3.07	2.75	3.22	2.3	3.23	3.84	3.66
SI7	4.56	5.07	2.84	6.45	1.75	6.15	6.49	6.43	7.51
SI8	6.21	6.31	2.07	5.73	5.23	5.96	5.13	5.48	6.55
SI9	5.65	4.47	3.38	6.68	5.12	6.02	6.92	6.85	7.42
SI10	6.19	6.15	6.42	6.76	6.06	6.24	6.23	6.49	6.55

Table 10
NIQE values obtained from various CE methods for the sample images.

Methods/ Images	EEBHE (2019)	JHE (2019)	LIME (2017)	STRU (2018)	LLnet (2018)	MIRnet (2020)	EGAN (2021)	Proposed
SI1	3.50	4.48	3.73	4.15	3.50	5.19	3.81	3.49
SI2	4.46	7.1	3.70	5.38	3.53	5.77	4.62	3.99
SI3	4.73	7.14	3.95	4.47	3.86	3.94	3.81	3.75
SI4	2.96	6.31	2.82	2.89	2.58	2.94	2.79	2.72
SI5	3.95	5.81	4.16	5.02	4.24	4.91	4.45	3.95
SI6	5.68	8.13	5.76	7.79	7.41	5.14	5.38	6.35
SI7	8.15	9.92	8.43	3.64	6.29	4.56	5.89	4.4
SI8	3.65	3.21	3.85	4.21	3.29	3.57	3.92	3.12
SI9	3.42	6.03	3.57	4.66	3.73	3.07	3.39	2.81
SI10	3.17	5.13	3.85	4.02	3.66	3.58	3.23	3.09

Table 11
Computed average values of REC for different CE methods applied on various databases.

Methods/ Databases	EEBHE (2019)	JHE (2019)	LIME (2017)	STRU (2018)	LLnet (2018)	MIRnet (2021)	EGAN (2021)	Proposed
CEED	1.002	0.99	1.000	0.9544	0.99	0.996	0.97	1.002
CSIQ	1.02	1.14	1.09	0.919	1.06	0.99	1.004	1.14
LOL	1.48	1.67	1.84	1.42	1.43	1.66	1.515	1.77
TID2013	1.04	1.06	1.04	0.97	1.01	1.083	1.006	1.087

Table 12
Computed average values of CIR for different CE methods applied on various databases.

Methods/ Databases	EEBHE (2019)	JHE (2019)	LIME (2017)	STRU (2018)	LLnet (2018)	MIRnet (2021)	EGAN (2021)	Proposed
CEED	1.55	1.36	0.19	0.23	0.15	2.22	1.414	2.343
CSIQ	0.14	8.76	0.13	0.14	0.127	0.826	0.421	10.06
LOL	1.89	1.69	1.37	0.71	0.826	0.818	0.901	1.94
TID2013	0.86	1.01	0.22	0.256	0.192	1.19	0.180	1.27

Table 13
Computed average values of SF for different CE methods applied on various databases.

Methods/ Databases	Input	EEBHE (2019)	JHE (2019)	LIME (2017)	STRU (2018)	LLnet (2018)	MIRnet (2021)	EGAN (2021)	Proposed
CEED	10.94	8.14	6.69	6.82	7.26	6.13	7.8	11.5	13.94
CSIQ	8.37	12.46	16.54	17.11	13.994	11.59	9.83	22.42	31.66
LOL	12.26	10.57	18.337	15.68	2.44	4.20	13.50	13.51	19.56
TID2013	21.95	23.13	21.33	18.10	20.17	22.35	26.50	25.76	26.05

EGAN give higher AMBE values, demonstrating a considerable deviation in the average luminance, whereas the proposed method preserves the average brightness and results in lower AMBE values due to the employment of histogram segmentation using the median value in comparison with methods available in the literature.

Table 9 presents the DE value of the enhanced images obtained from the existing methodologies, including the suggested method. As seen from the table, the suggested approach has a higher DE value than the other algorithms, with the exception of SI6. It indicates that the proposed method improves images while maximizing the information content. Entropy values the images obtained from EEBHE are less than

those of the input indicates that information is lost throughout the enhancement process. This could be attributable to the histogram clipping performed by these methods. Lower entropy values are obtained for the images produced from the JHE. It is due to the merging of intensities during the transformation process. The table demonstrates that the illumination based techniques and the CNN architectures maintain information integrity during augmentation. Utilizing structural information derived from Rényi entropy aids in preserving and maximizing the image's information, which may help to produce a high DE value for the suggested method.

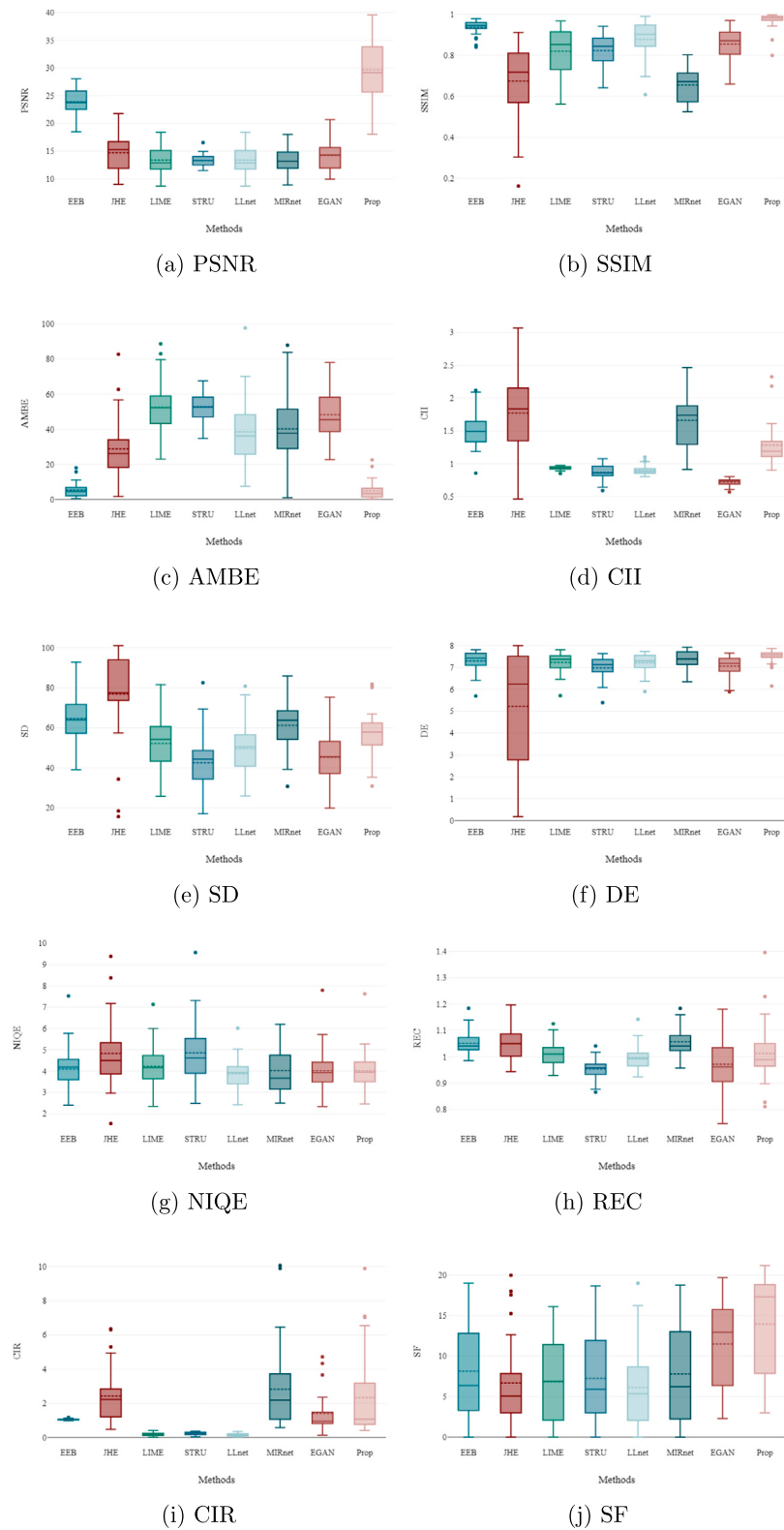


Fig. 14. Boxplot of various performance measures for CEED database.

Table 10 displays the NIQE values of the example images produced using the approaches provided in the existing and the proposed algorithm. NIQE is a no reference performance measure to quantify the amount of visual degradation. It has a close connection to human judgments. As shown in **Table 10**, compared to other techniques, the suggested methodology has a low NIQE except three sample images.

It indicates that the suggested method yields a improved image with minimum artifacts.

Fig. 14 shows the box plots of various metric values for contrast enhancement techniques obtained on the CEED database. **Fig. 14(a)** represents the PSNR for various techniques available in the literature along with the proposed method. The proposed technique produces the

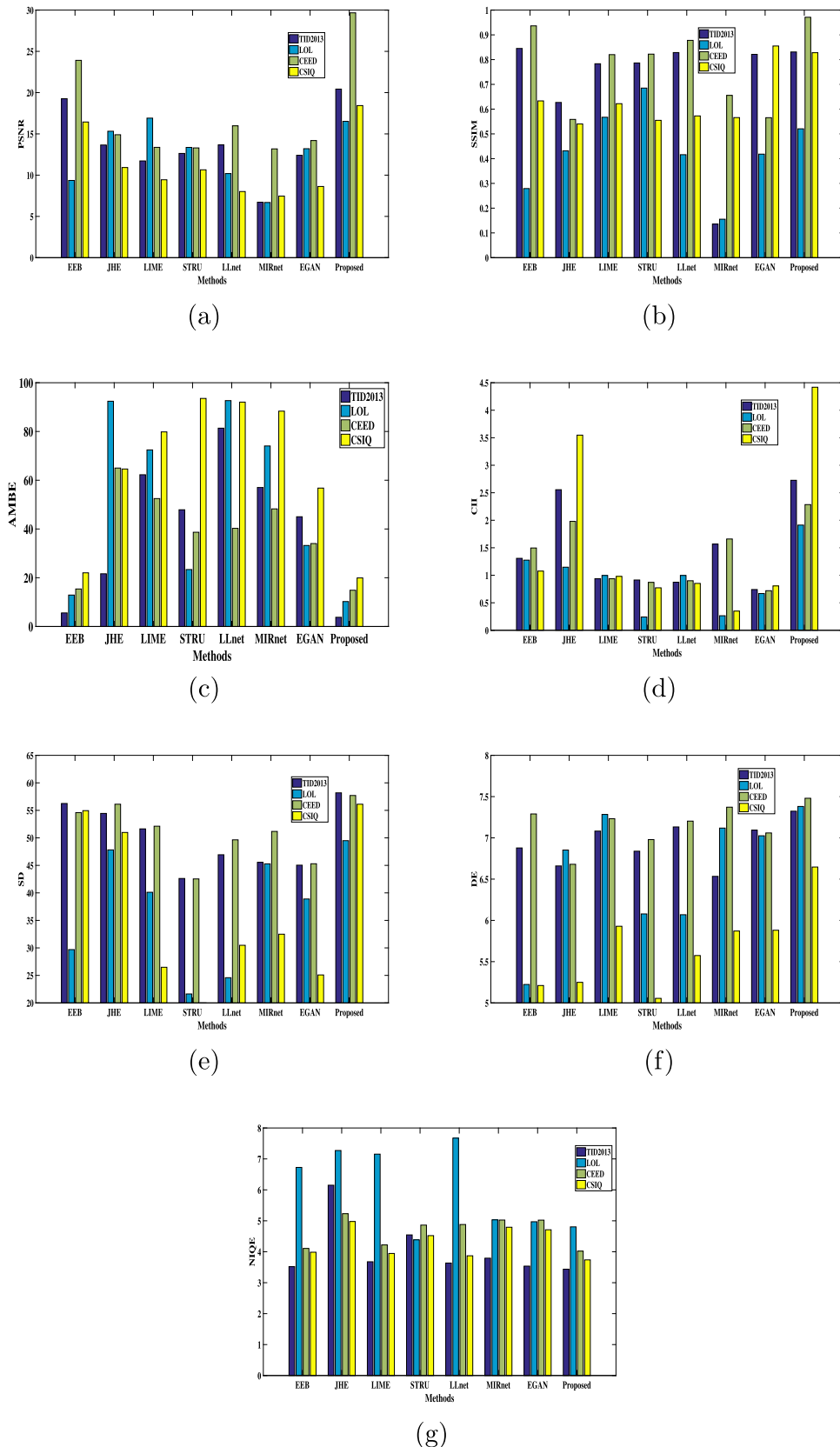


Fig. 15. Graphical representation of the mean values various performance measures for different databases: (a) PSNR, (b) SSIM, (c) AMBE, (d) CII, (e) SD, (f) DE, and (g) NIQE.

highest PSNR value and spread for a wider range. Fig. 14(b) shows the SSIM value for the enhancement techniques. It is observed that the proposed method results in a high SSIM value and it is dispersed in

low range of values. Fig. 14(c) and Fig. 14(d) show the CII and SD values for the various methods respectively. It is observed from the Figure that CII and SD values are less dispersed when compared to

Table 14

Average processing time period for various enhancement techniques.

Databases	Average time period in sec							
	EEBHE	JHE	LIME	STRU	LLnet	MIRnet	EGAN	Proposed
TID 2013	1.26	8.62	0.24	5.93	2.25	3.01	1.44	1.21
LOL	1.01	9.54	0.23	7.33	2.72	3.32	1.04	0.98
CEED	1.40	14.93	0.94	9.37	2.83	4.02	2.58	1.48
CSIQ	1.20	13.82	0.21	9.34	2.79	3.75	1.28	1.07

the other existing techniques. Fig. 14(e) shows box plot of DE value of different contrast enhancement techniques, and it is seen that the proposed method results in high DE value with less dispersion. AMBE and NIQE values are shown in Fig. 14(f) and Fig. 14(g). It is inferred from the figures that the lowest values of NIQE and AMBE are obtained by the proposed method compared to the other techniques. Fig. 14(h) and Fig. 14(i) show the REC and CIR values of the CEED database obtained by different enhancement techniques. From the box plot, it is observed that the proposed technique produced high CIR and REC values with less dispersion. Fig. 14(j) shows the SF value and it is inferred from the box plot that the suggested technique results in a high SF value. It can be observed that the proposed method produces less dispersed metric values for SSIM, CII, SD, DE, AMBE, NIQE and REC. The proposed technique follows the similar dispersion of NIQE and SF with the EGAN. It may be concluded that, the proposed Rényi entropy-based method enhances the image by increasing the differences between the neighborhood indicated by the high CIR, REC, CII and SD values. It preserves the information content well compared to the other existing techniques indicated by the high DE and SF values and also the proposed method results in artifact free enhanced images indicated by the low AMBE and NIQE values.

Fig. 15 depicts a bar chart of the mean values of various performance measures obtained from four datasets. The graph demonstrates that the suggested technique produces the maximum CII, SD, and DE values across all databases, while achieving the least NIQE and AMBE values in comparison with the methods available in the literature. These results indicate that the suggested Rényi entropy based approach enhances the degraded images by increasing the contrast and maintains information content in the processed image more effectively than existing methods.

Table 11 shows the mean REC value for different contrast enhancement (CE) techniques obtained on various databases. The proposed technique produces the highest REC for three databases (CEED, CSIQ and TID2013). The higher REC value indicates the improvement in contrast of the image compared to the existing methods in the literature. The mean CIR value for various contrast enhancement (CE) approaches, as determined from various databases, is shown in Table 12. For all databases, the suggested method yields the highest CIR. In comparison to the approaches already in the literature, the image's local contrast is improved as indicated by the higher CIR value. Table 13 displays the mean SF value for several CE techniques as derived from various databases. The suggested strategy produces the highest SF across all databases. The greater SF value shows that the spatial information of the image is improved in compared to methods already described in the literature due to the employment of the local contrast improvement using discrete cosine transform.

Table 14 shows the average time process period for the databases used for evaluation of the proposed methodology along with methods existing in the literature. From the table it is observed that, LIME produces the enhanced image in a shorter time period when compared to the other methods. The proposed methodology stands at the second position for all the databases in the average execution time period. The execution time period is varied based on the size of the images and the number of unique intensities present in the image.

4.4. Statistical analysis

The Wilcoxon Signed Rank Test [61] is conducted for statistical analysis and performed using non-parametric tests. The Wilcoxon Signed Rank Test is used to make paired observations, taking as the pairs the outcomes of each algorithm in relation to the proposed method [62]. Table 15 displays the results of the Wilcoxon Signed Rank Test. The null hypothesis for the Wilcoxon signed rank test is that both samples come from the same population. A pooled ranking of all observed differences between the two dependent metrics is produced by the Wilcoxon test. The usual normal distributed z-value is employed to test for significance. In essence, the tests compute the difference between groups of pairings and examine this difference to determine whether it is statistically significant. If the p-value is nearly zero, then the null hypothesis will be rejected and If the z values are lesser than -1.96 or greater than 1.96 then the null hypothesis will be rejected.

From Table 15, it is observed that, the proposed methodology is significantly better to the existing algorithms in terms of PSNR and SSIM. For the AMBE metric, the proposed method results in better values in comparison with the existing techniques excluding EEBHE technique. It can be inferred that the proposed algorithm preserves the mean brightness of the enhanced images. DE and SF values are significantly high for the proposed method compared to the existing methods in the literature. They indicate that the proposed methodology preserves the information content and retains the spatial information of the improved images. Compared to existing approaches in the literature, the proposed method has much higher SD and REC values indicating the global contrast improvement of the resultant images. CII and CIR are significantly high for the suggested technique compared to the other techniques implying local contrast improvement of the processed images. From the above statistical analysis, it may be concluded that, the image is improved by the suggested Rényi entropy-based technique by boosting the differences between the neighborhood denoted by the high CIR, REC, CII, and SD values. The high DE and SF values show that it outperforms other existing strategies at preserving information content, while the low AMBE and NIQE values show that the proposed method produces artifact-free enhanced images.

5. Conclusion

This research proposes a contrast enhancement technique based on structural information to improve the quality of the uniform background images. The presence of histogram spikes in the homogeneous background images cause mean brightness shifting and over enhancement, producing halo artifacts in the enhanced image. The statistical parameter median divides the intensity values into two segments to preserve the average luminance. The image's histogram is computed concerning the structural locations by dividing the image into the number of the structural grid. Rényi entropy is calculated for each intensity value to incorporate the structural information in the equalization process. Employment of adaptive clipping limit controls the enhancement level by considering the minimum value among the discrete function's mean, median, and discrete value. Clipped discrete functions are equalized separately and integrated to produce an improved image. Discrete cosine transformation enhances the contrast of the improved image in local regions. Experimental analysis shows that the proposed

Table 15

Wilcoxon signed test for the various metrics computed on CEED database.

Metrics/Methods	Testvalues	PSNR	SSIM	AMBE	CII	SD	DE	NIQE	REC	CIR	SF
Proposedand EEBHE	Positive	26	26	12	6	7	22	13	14	16	21
	Negative	4	4	18	24	23	8	17	16	14	9
	z	-4	-3.82	-0.94	-2.93	-3.28	-3.32	-0.81	-0.75	-1.51	-3.14
	p-value	0.001	0.001	0.35	0.03	0.001	<0.001	0.417	0.453	0.137	0.002
Proposedand JHE	Positive	30	30	1	4	4	22	6	22	21	26
	Negative	0	0	29	26	26	8	24	8	9	4
	z	-4.78	-4.78	-4.76	-3.61	-3.53	-3.61	-3.26	-2.36	-1.414	-3.9
	p-value	0.001	0.001	0.001	<0.001	<0.001	<0.001	0.001	0.019	0.254	<0.001
Proposedand LIME	Positive	30	29	0	29	24	24	10	16	30	22
	Negative	0	1	30	1	6	6	20	14	0	8
	z	-4.78	-4.41	-4.78	-4.74	-3.01	-3.22	-1.98	-0.75	-4.78	-3.51
	p-value	0.001	<0.001	0.001	<0.001	0.003	0.001	0.047	0.453	<0.001	<0.001
Proposedand STRU	Positive	30	29	0	30	27	27	3	21	30	26
	Negative	0	1	30	0	3	3	27	9	0	4
	z	-4.78	-4.58	-4.78	-4.78	-4.66	-4.49	-4.37	-2.54	-4.78	-4.12
	p-value	0.001	<0.001	0.001	<0.001	<0.001	<0.001	<0.001	0.011	<0.001	<0.001
Proposed and LLnet	Positive	30	28	0	29	25	24	18	16	30	26
	Negative	0	2	30	1	5	6	12	14	0	4
	z	-4.78	-4.19	-4.78	-4.76	-3.65	-3.53	-1.61	-0.67	-4.78	-4.35
	p-value	0.001	<0.001	0.001	<0.001	<0.001	<0.001	0.106	0.55	<0.001	<0.001
Proposedand MIRnet	Positive	30	30	0	5	12	15	14	20	20	24
	Negative	0	0	30	25	18	15	16	10	10	6
	z	-4.78	-4.78	-4.78	-3.69	-1.55	-1.04	-0.55	-2.23	-1.14	-3.14
	p-value	0.001	<0.001	0.001	<0.001	0.12	0.209	0.586	0.026	0.025	0.002
Proposedand EGAN	Positive	30	28	0	30	24	23	15	19	16	20
	Negative	0	2	30	0	6	7	15	11	14	10
	z	-4.78	-4.7	-4.78	-4.78	-3.26	-3.36	-0.26	-1.2	-0.84	-1.66
	p-value	0.001	<0.001	0.001	<0.001	0.001	0.001	0.797	0.229	0.382	0.098

methodology produces high CII and SD values, indicating an improvement in the contrast. It results in high DE, SSIM, and PSNR specifying the preservation of information. The low AMBE and NIQE values imply the reduction in visual artifacts compared to the other methods existing in the literature, including deep learning architectures. This method could be used as a pre-processing step to increase the performance of computer vision tasks like object recognition and classification.

CRediT authorship contribution statement

D. Vijayalakshmi: Conceptualization, Methodology/Study design, Software, Validation, Resources, Data curation, Writing – original draft. **Malaya Kumar Nath:** Formal analysis, Investigation, Writing – review & editing, Visualization, Supervision.

Declaration of competing interest

The authors declare that they have no known competing financial interests or personal relationships that could have appeared to influence the work reported in this paper.

Data availability

Data will be made available on request.

References

- [1] G. Zhang, X. Jia, N.M. Kwok, Super pixel based remote sensing image classification with histogram descriptors on spectral and spatial data, in: 2012 IEEE International Geoscience and Remote Sensing Symposium, 2012, pp. 4335–4338, <http://dx.doi.org/10.1109/IGARSS.2012.6351708>.
- [2] H. Ma, N. Lu, L. Ge, Q. Li, X. You, X. Li, Automatic road damage detection using high-resolution satellite images and road maps, in: 2013 IEEE International Geoscience and Remote Sensing Symposium, IGARSS, 2013, pp. 3718–3721, <http://dx.doi.org/10.1109/IGARSS.2013.6723638>.
- [3] J. Bruce, T. Balch, M. Veloso, Fast and inexpensive color image segmentation for interactive robots, in: Proceedings. 2000 IEEE/RSJ International Conference on Intelligent Robots and Systems (IROS 2000) (Cat. No.00CH37113), Vol. 3, 2000, pp. 2061–2066, <http://dx.doi.org/10.1109/IROS.2000.895274>.
- [4] B. Huang, T. Xu, S. Jiang, Y. Chen, Y. Bai, Robust visual tracking via constrained multi-kernel correlation filters, *IEEE Trans. Multimed.* 22 (11) (2020) 2820–2832, <http://dx.doi.org/10.1109/TMM.2020.2965482>.
- [5] G. Varol, I. Laptev, C. Schmid, Long-term temporal convolutions for action recognition, *IEEE Trans. Pattern Anal. Mach. Intell.* 40 (6) (2018) 1510–1517, <http://dx.doi.org/10.1109/TPAMI.2017.2712608>.
- [6] J. Li, X. Liang, J. Li, Y. Wei, T. Xu, J. Feng, S. Yan, Multistage object detection with group recursive learning, *IEEE Trans. Multimed.* 20 (7) (2018) 1645–1655, <http://dx.doi.org/10.1109/TMM.2017.2772796>.
- [7] P. Zhuang, X. Ding, Underwater image enhancement using an edge-preserving filtering retinex algorithm, *Multimedia Tools Appl.* 79 (25) (2020) 17257–17277.
- [8] H. Moftah, A. Azar, E. Al-Shammari, N. Ghali, A.E. Hassani, M. Shoman, Adaptive k-means clustering algorithm for MR breast image segmentation, *Neural Comput. Appl.* 24 (2013) <http://dx.doi.org/10.1007/s00521-013-1437-4>.
- [9] L. Dong, W. Zhang, W. Xu, Underwater image enhancement via integrated RGB and LAB color models, *Signal Process., Image Commun.* 104 (2022) 116684.
- [10] D. Vijayalakshmi, M.K. Nath, O.P. Acharya, A comprehensive survey on image contrast enhancement techniques in spatial domain, *Sens. Imaging* 21 (2020) 1–40, <http://dx.doi.org/10.1007/s11220-020-00305-3>.
- [11] D. Vijayalakshmi, M.K. Nath, A novel multilevel framework based contrast enhancement for uniform and non-uniform background images using a suitable histogram equalization, *Digit. Signal Process.* 127 (2022) 1–19.
- [12] Y.C. Hum, Y.K. Tee, W.-S. Yap, H. Mokayed, T.S. Tan, M.I.M. Salim, K.W. Lai, A contrast enhancement framework under uncontrolled environments based on just noticeable difference, *Signal Process., Image Commun.* 103 (2022) 116657.
- [13] D. Vijayalakshmi, M.K. Nath, A novel contrast enhancement technique using gradient-based joint histogram equalization, *Circuits Syst. Signal Process.* 40 (2021) 3929–3967, <http://dx.doi.org/10.1007/s00034-021-01655-3>.
- [14] X. Wang, L. Chen, An effective histogram modification scheme for image contrast enhancement, *Signal Process., Image Commun.* 58 (2017) 187–198.
- [15] V. Dhurairajan, P. Elangovan, M.K. Nath, Renyi entropy based bi-histogram equalization for contrast enhancement of MRI brain images, in: NIScPR-CSIR, India, 2021.
- [16] D. Vijayalakshmi, M.K. Nath, A compendious analysis of advances in HE methods for contrast enhancement, in: Advances in VLSI, Communication, and Signal Processing, Springer, 2021, pp. 325–346, http://dx.doi.org/10.1007/978-981-15-6840-4_26.
- [17] K. Zuiderveld, Contrast limited adaptive histogram equalization, in: P.S. Heckbert (Ed.), *Graphics Gems*, Academic Press, 1994, pp. 474–485.
- [18] Y.-T. Kim, Contrast enhancement using brightness preserving bi-histogram equalization, *IEEE Trans. Consum. Electron.* 43 (1) (1997) 1–8, <http://dx.doi.org/10.1109/30.580378>.
- [19] Y. Wang, Q. Chen, B. Zhang, Image enhancement based on equal area dualistic sub-image histogram equalization method, *IEEE Trans. Consum. Electron.* 45 (1) (1999) 68–75, <http://dx.doi.org/10.1109/30.754419>.

- [20] S.-D. Chen, A.R. Ramli, Contrast enhancement using recursive mean-separate histogram equalization for scalable brightness preservation, *IEEE Trans. Consum. Electron.* 49 (4) (2003) 1301–1309, <http://dx.doi.org/10.1109/TCE.2003.1261233>.
- [21] C.H. Ooi, N.S.P. Kong, H. Ibrahim, Bi-histogram equalization with a plateau limit for digital image enhancement, *IEEE Trans. Consum. Electron.* 55 (4) (2009) 2072–2080, <http://dx.doi.org/10.1109/TCE.2009.5373771>.
- [22] J.R. Tang, N.A.M. Isa, Adaptive image enhancement based on bi-histogram equalization with a clipping limit, *Comput. Electr. Eng.* 40 (8) (2014) 86–103, <http://dx.doi.org/10.1016/j.compeleceng.2014.05.017>.
- [23] X. Wang, L. Chen, Contrast enhancement using feature-preserving bi-histogram equalization, *Signal Image Video Process.* 12 (4) (2018) 685–692, <http://dx.doi.org/10.1007/s11760-017-1208-2>.
- [24] J. Mun, Y. Jang, Y. Nam, J. Kim, Edge-enhancing bi-histogram equalisation using guided image filter, *J. Vis. Commun. Image Represent.* 58 (2019) 688–700, <http://dx.doi.org/10.1016/j.jvcir.2018.12.037>.
- [25] T. Celik, Spatial entropy-based global and local image contrast enhancement, *IEEE Trans. Image Process.* 23 (12) (2014) 5298–5308, <http://dx.doi.org/10.1109/TIP.2014.2364537>.
- [26] T. Celik, H.-C. Li, Residual spatial entropy-based image contrast enhancement and gradient-based relative contrast measurement, *J. Modern Opt.* 63 (16) (2016) 1600–1617, <http://dx.doi.org/10.1080/09500340.2016.1163427>.
- [27] C. Lee, C. Lee, C. Kim, Contrast enhancement based on layered difference representation of 2D histograms, *IEEE Trans. Image Process.* 22 (12) (2013) 5372–5384, <http://dx.doi.org/10.1109/TIP.2013.2284059>.
- [28] M. Veluchamy, B. Subramani, Image contrast and color enhancement using adaptive gamma correction and histogram equalization, *Optik* 183 (2019) 329–337.
- [29] S. Agrawal, R. Panda, P. Mishra, A. Abraham, A novel joint histogram equalization based image contrast enhancement, *J. King Saud Univ. - Comput. Inf. Sci.* (2019) <http://dx.doi.org/10.1016/j.jksuci.2019.05.010>.
- [30] H. Rahman, G.C. Paul, Tripartite sub-image histogram equalization for slightly low contrast gray-tone image enhancement, *Pattern Recognit.* 134 (2023) 109043.
- [31] X. Fu, D. Zeng, Y. Huang, Y. Liao, X. Ding, J. Paisley, A fusion-based enhancing method for weakly illuminated images, *Signal Process.* 129 (2016) 82–96, <http://dx.doi.org/10.1016/j.sigpro.2016.05.031>.
- [32] X. Fu, D. Zeng, Y. Huang, X.-P. Zhang, X. Ding, A weighted variational model for simultaneous reflectance and illumination estimation, in: 2016 IEEE Conference on Computer Vision and Pattern Recognition, CVPR, 2016, pp. 2782–2790, <http://dx.doi.org/10.1109/CVPR.2016.304>.
- [33] X. Guo, Y. Li, H. Ling, LIME: Low-light image enhancement via illumination map estimation, *IEEE Trans. Image Process.* 26 (2) (2017) 982–993, <http://dx.doi.org/10.1109/TIP.2016.2639450>.
- [34] M. Li, J. Liu, W. Yang, X. Sun, Z. Guo, Structure-revealing low-light image enhancement via robust retinex model, *IEEE Trans. Image Process.* 27 (6) (2018) 2828–2841, <http://dx.doi.org/10.1109/TIP.2018.2810539>.
- [35] L. Maurya, V. Lohchab, P. Kumar Mahapatra, J. Abonyi, Contrast and brightness balance in image enhancement using cuckoo search-optimized image fusion, *J. King Saud Univ. - Comp. Inf. Sci.* 34 (9) (2022) 7247–7258.
- [36] R. Liu, S. Cheng, L. Ma, X. Fan, Z. Luo, Deep proximal unrolling: Algorithmic framework, convergence analysis and applications, *IEEE Trans. Image Process.* 28 (10) (2019) 5013–5026, <http://dx.doi.org/10.1109/TIP.2019.2913536>.
- [37] H. Zhang, V.M. Patel, Density-aware single image de-raining using a multi-stream dense network, in: 2018 IEEE/CVF Conference on Computer Vision and Pattern Recognition, 2018, pp. 695–704, <http://dx.doi.org/10.1109/CVPR.2018.00079>.
- [38] T.-W. Hui, X. Tang, C.C. Loy, LiteFlowNet: A lightweight convolutional neural network for optical flow estimation, in: 2018 IEEE/CVF Conference on Computer Vision and Pattern Recognition, 2018, pp. 8981–8989, <http://dx.doi.org/10.1109/CVPR.2018.00936>.
- [39] C. Wei, W. Wang, W. Yang, J. Liu, Deep retinex decomposition for low-light enhancement, in: British Machine Vision Conference, 2018.
- [40] C. Li, J. Guo, F. Porikli, Y. Pang, LightenNet: A convolutional neural network for weakly illuminated image enhancement, *Pattern Recognit. Lett.* 104 (2018) 15–22, <http://dx.doi.org/10.1016/j.patrec.2018.01.010>.
- [41] Y. Jiang, X. Gong, D. Liu, Y. Cheng, C. Fang, X. Shen, J. Yang, P. Zhou, Z. Wang, EnlightenGAN: Deep light enhancement without paired supervision, *IEEE Trans. Image Process.* 30 (2021) 2340–2349, <http://dx.doi.org/10.1109/TIP.2021.3051462>.
- [42] S.W. Zamir, A. Arora, S. Khan, M. Hayat, F.S. Khan, M.-H. Yang, L. Shao, Learning enriched features for real image restoration and enhancement, 2020, pp. 1–20, [arXiv:2003.06792](https://arxiv.org/abs/2003.06792).
- [43] V. Dhurairajan, T.S. Kumari, C.A. Bhavani, Low contrast image enhancement using renyi entropy, *Sci. Technol. Res. Inst. Def. (STRIDE)* 11 (2018) 113–122.
- [44] X. Fu, X. Cao, Underwater image enhancement with global-local networks and compressed-histogram equalization, *Signal Process., Image Commun.* 86 (2020) 115892.
- [45] M.E. Reddy, G.R. Reddy, Recursive median and mean partitioned one-to-one gray level mapping transformations for image enhancement, *Circuits Systems Signal Process.* (2019).
- [46] O. Chen Hee, New Histogram Equalization Based Detail and Brightness Preserving Techniques for Digital Images (Master's thesis), Universiti Sains Malaysia, 2010.
- [47] N. Ponomarenko, L. Jin, O. Ieremeiev, V. Lukin, K. Egiazarian, J. Astola, B. Vozel, K. Chehdi, M. Carli, F. Battisti, C.-C. Jay Kuo, Image database TID2013: Peculiarities, results and perspectives, *Signal Process., Image Commun.* 30 (2015) 57–77, <http://dx.doi.org/10.1016/j.image.2014.10.009>.
- [48] URL <http://r0k.us/graphics/kodak/>.
- [49] E. Larson, D. Chandler, Most apparent distortion: Full-reference image quality assessment and the role of strategy, *J. Electron. Imaging* 19 (1) (2010) 1–21, <http://dx.doi.org/10.1117/1.3267105>.
- [50] C. Wei, W. Wang, W. Yang, J. Liu, Deep retinex decomposition for low-light enhancement, 2018, [arXiv:1808.04560](https://arxiv.org/abs/1808.04560).
- [51] M. Qureshi, A. Beghdadi, M. Deriche, Towards the design of a consistent image contrast enhancement evaluation measure, *Signal Process. Image Commun.* 58 (2017).
- [52] P. Zeng, H. Dong, J. Chi, X. Xu, An approach for wavelet based image enhancement, in: 2004 IEEE International Conference on Robotics and Biomimetics, 2004, <http://dx.doi.org/10.1109/ROBIO.2004.1521843>.
- [53] C.E. Shannon, A mathematical theory of communication, *Bell Syst. Tech. J.* 27 (3) (1948) 379–423, <http://dx.doi.org/10.1002/j.1538-7305.1948.tb01338.x>.
- [54] Z. Wang, A.C. Bovik, H.R. Sheikh, E.P. Simoncelli, Image quality assessment: from error visibility to structural similarity, *IEEE Trans. Image Process.* 13 (4) (2004) 600–612, <http://dx.doi.org/10.1109/TIP.2003.819861>.
- [55] R.C. González, R.E. Woods, *Digital Image Processing*, third ed., Pearson Education, 2008.
- [56] A. Mittal, R. Soundararajan, A.C. Bovik, Making a “Completely Blind” image quality analyzer, *IEEE Signal Process. Lett.* 20 (3) (2013) 209–212, <http://dx.doi.org/10.1109/LSP.2012.2227726>.
- [57] D. Vijayalakshmi, M.K. Nath, Taxonomy of performance measures for contrast enhancement, *Pattern Recognit. Image Anal.* 30 (2021) 691–701, <http://dx.doi.org/10.1134/S1054661820040240>.
- [58] J. Joseph, R. Periyasamy, A fully customized enhancement scheme for controlling brightness error and contrast in magnetic resonance images, *Biomed. Signal Process. Control* 39 (2018) 271–283.
- [59] Y.-P. Wang, Q. Wu, K.R. Castleman, Z. Xiong, Chromosome image enhancement using multiscale differential operators, *IEEE Trans. Med. Imaging* 22 (5) (2003) 685–693.
- [60] R. Shapley, P. Lennie, Spatial frequency analysis in the visual system, *Annu. Rev. Neurosci.* 8 (1) (1985) 547–581.
- [61] F. Wilcoxon, *Individual Comparisons By Ranking Methods*, Springer, 1992.
- [62] J.C.M. Román, V.R. Fretes, C.G. Adorno, R.G. Silva, J.L.V. Noguera, H. Legal-Ayala, J.D. Mello-Román, R.D.E. Torres, J. Facon, Panoramic dental radiography image enhancement using multiscale mathematical morphology, *Sensors* 21 (9) (2021).